JGR Atmospheres

RESEARCH ARTICLE
10.1029/2023JD038618

Performance of Regional Climate Model Precipitation Simulations Over the Terrain-Complex Andes-Amazon Transition Region

Ricardo A. Gutierrez[1,2], Clémentine Junquas[3,4], Elisa Armijos[1,2], Anna A. Sörensson[5,6,7], and Jhan-Carlo Espinoza[3,8]

[1]Escuela de Posgrado, Universidad Nacional Agraria La Molina, Lima, Perú, [2]Subdirección de Ciencias de la Atmósfera e Hidrósfera, Instituto Geofísico del Perú, Lima, Perú, [3]Univ. Grenoble Alpes, IRD, CNRS, INRAE, Grenoble INP, IGE, Grenoble, France, [4]Servicio Nacional de Meteorología e Hidrología (SENAMHI), Lima, Peru, [5]Facultad de Ciencias Exactas y Naturales, Universidad de Buenos Aires, Buenos Aires, Argentina, [6]Centro de Investigaciones del Mar y la Atmósfera (CIMA), CONICET – Universidad de Buenos Aires, Buenos Aires, Argentina, [7]Instituto Franco-Argentino de Estudios sobre el Clima y sus Impactos (IFAECI - IRL 3351), CNRS-CONICET-IRDUBA, Buenos Aires, Argentina, [8]Departamento de Ciencias, Sección Matemáticas, Pontificia Universidad Católica del Perú, Lima, Perú

Key Points:

- Precipitation output from 30 regional climate simulations is assessed over the Andes-Amazon in terms of climatology and temporal variability
- The spatio-temporal behavior of seasonality is well reproduced by most simulations, with overestimations during austral summer and spring
- While orographic precipitation is a major challenge for most regional climate models, Eta satisfactorily reproduces climate patterns in the Andes-Amazon region

Supporting Information:

Supporting Information may be found in the online version of this article.

Correspondence to:

R. A. Gutierrez,
ra.gvillarreal@gmail.com

Citation:

Gutierrez, R. A., Junquas, C., Armijos, E., Sörensson, A. A., & Espinoza, J.-C. (2024). Performance of regional climate model precipitation simulations over the terrain-complex Andes-Amazon transition region. *Journal of Geophysical Research: Atmospheres*, *129*, e2023JD038618. https://doi.org/10.1029/2023JD038618

Received 2 FEB 2023
Accepted 28 NOV 2023

Abstract Regional climate models (RCMs) are widely used to assess future impacts associated with climate change at regional and local scales. RCMs must represent relevant climate variables in the present-day climate to be considered fit-for-purpose for impact assessment. This condition is particularly difficult to meet over complex regions such as the Andes-Amazon transition region, where the Andean topography and abundance of tropical rainfall regimes remain a challenge for numerical climate models. In this study, we evaluate the ability of 30 regional climate simulations (6 RCMs driven by 10 global climate models) to reproduce historical (1981–2005) rainfall climatology and temporal variability over the Andes-Amazon transition region. We assess spatio-temporal features such as spatial distribution of rainfall, focusing on the orographic effects over the Andes-Amazon "rainfall hotspots" region, and seasonal and interannual precipitation variability. The Eta RCM exhibits the highest spatial correlation (up to 0.6) and accurately reproduces mean annual precipitation and orographic precipitation patterns across the region, while some other RCMs have good performances at specific locations. Most RCMs simulate a wet bias over the highlands, particularly at the eastern Andean summits, as evidenced by the 100%–2,500% overestimations of precipitation in these regions. Annual cycles are well represented by most RCMs, but peak seasons are exaggerated, especially at equatorial locations. No RCM is particularly skillful in reproducing the interannual variability patterns. Results highlight skills and weaknesses of the different regional climate simulations, and can assist in the selection of regional climate simulations for impact studies in the Andes-Amazon transition zone.

Plain Language Summary Regional climate models (RCMs) are useful numerical tools to investigate future climate change impacts (e.g., future water availability, frequency of floods and droughts, regional warming). Regarding regional scale, RCMs are expected to perform better than global climate models due to finer spatial resolution. However, in the Andes-Amazon transition region, assessing the performance of RCMs is challenging due to complex terrain and scarcity of observations. This region is of critical importance for the water cycle of local and regional ecological systems, but has been often overlooked in RCM assessments. Here, we evaluate how 30 regional climate simulations perform in representing precipitation regional contrasts, wet-dry seasons, and year-to-year changes over the Andes-Amazon transition region. We find that models perform differently over specific regions, with prominent overestimations at high altitudes by most RCMs. However, Eta RCM has the best performance regarding regional patterns of precipitation and its wet-dry fluctuations. Besides overestimations during austral summer and spring, wet-dry seasonal fluctuations are well simulated by most RCMs, but none excels in representing wet-dry yearly fluctuations. Strengths and weaknesses of different regional climate simulations are shown, and can help choose the most appropriate simulations for distinct impact studies in this region.

1. Introduction

Current and future hydroclimatic trajectories pose significant challenges to global socioeconomic and environmental systems, including fragile ecosystems (Pörtner et al., 2022). Hydroclimatic changes in the western Amazon

(0°–16°S and 80°W–69°W), including the Andes-Amazon transition region, are linked to the intensification of seasonal floods and droughts resulting from shifts in precipitation intensities (Arias et al., 2021; Espinoza et al., 2019, 2016; Haghtalab et al., 2020; Pabón-Caicedo et al., 2020). Anthropogenic climate and land-surface alterations also contribute to these changes (Marengo et al., 2018; Nobre et al., 2016). Global warming and deforestation have already disrupted the hydroclimatic functioning of ecosystems such as glaciers, paramos, rainforests, and montane cloud forests, which provide essential ecological services. Continued human-induced alterations are expected to exacerbate these impacts (Adler et al., 2022; Boulton et al., 2022; Ometto et al., 2022; Vuille et al., 2018; Young et al., 2011). This is of particular concern for the Andes-Amazon transition region, known as the rainiest and most biodiverse area within the Amazon basin (Espinoza et al., 2015; Hoorn et al., 2010). This region is a major source of sediment for the Amazon rivers and plays a crucial role in precipitation recycling within South America (Armijos et al., 2020; Staal et al., 2018). Therefore, there is a pressing need for future precipitation projections much needed to inform the development of adaptation policies and strategies for addressing climate change in this region.

Global climate models (GCMs) are widely recognized as essential tools for studying future climate change, with their simulations being coordinated through the Coupled Model Intercomparison Projects (CMIP3, CMIP5, and CMIP6; Eyring et al., 2016; Meehl et al., 2007; Taylor et al., 2012, respectively). However, GCMs have limitations due to their relatively coarse spatial resolution, which results in an inability to capture many local and sub-regional processes. This limitation is particularly pronounced in the Andes-Amazon transition region, given its complex orography and the associated mesoscale circulation processes that cannot be adequately represented by these coarse grids. Consequently, these models often struggle to accurately depict the precipitation climatology in this region, frequently leading to substantial overestimations across the tropical Andes (Almazroui et al., 2021; Ortega et al., 2021). In this context, this bias in precipitation is notable, with values consistently exceeding 200% throughout the year (Ortega et al., 2021).

Regional climate models (RCMs) are frequently employed as dynamic downscaling tools for GCMs, aiming to provide more detailed climate information by better capturing topographical and land-surface heterogeneities (Ambrizzi et al., 2019; Giorgi & Gutowski, 2015). Notably, the Coordinated Regional Downscaling Experiment (CORDEX; Giorgi & Gutowski, 2015) has established a unified framework for conducting regional climate simulations worldwide, including South America (CORDEX-SAM).

However, it is important to note that many CORDEX simulations exhibit biases similar to those of GCMs, such as the substantial overestimation of mean summer precipitation along the tropical Andes, often exceeding observed amounts by a factor of two or more (Chou et al., 2014; Menéndez et al., 2016; Solman & Blázquez, 2019). Nevertheless, RCMs of the CORDEX-type hold the potential to enhance the representation of precipitation climatological fields in regions characterized by complex topography (Bozkurt et al., 2019; Prein et al., 2016; Torma et al., 2015).

Projections of future precipitation changes generated by CORDEX-SAM RCMs generally align with some aspects of GCM projections in the Amazon and the Andes, including increased summer precipitation in the tropical Andes and drier conditions in southwestern Amazonia. However, it is important to emphasize that the magnitude and directions of these changes vary depending on the specific RCM used (e.g., Blázquez & Solman, 2020; Llopart et al., 2019; Reboita et al., 2022).

The Andes-Amazon transition region features intricate precipitation patterns influenced by the interplay of large-scale and local circulation patterns and the region's physio-geographical characteristics (Espinoza et al., 2020 and references therein). Precipitation patterns across the western Amazon basin typically exhibit a seasonal distribution, although some Peruvian and Ecuadorian Amazon basins display unimodal and bimodal regimes (Espinoza et al., 2009; Laraque et al., 2007; Segura et al., 2019; J. C. Sulca and Rocha, 2021).

Within the equatorial Amazon basin, a notable rainfall peak occurs during March to May (MAM), corresponding to the southward movement of the Intertropical Convergence Zone (ITCZ). Another peak is observed in October and November, associated with the westward transport of moisture linked to the initiation of the South American Monsoon System (SAMS) (Vera et al., 2006).

In the central and southern Peruvian Amazon, a marked rainy season occurs during the austral summer, spanning from December to March, and is closely linked to the mature phase of the SAMS. Conversely, the dry season prevails from May to September. Furthermore, maximum precipitation regions, often referred to as

rainfall hotspots, are concentrated along the eastern slopes of the Andes (Chavez & Takahashi, 2017; Espinoza et al., 2015). These rainfall hotspots result from forced convection caused by to the orographic effect of the Andes (e.g., Eghdami & Barros, 2020; Garreaud, 2009; Junquas et al., 2018).

Therefore, the substantial diversity of rainfall regimes, stemming from the complex orographic features, renders regional climate modeling in the Andes-Amazon transition region a particularly challenging endeavor. However, it is worth noting that these challenges are compounded with uncertainties associated with observational data, including both satellite and gauge-based products, as well as the limited availability of observations in the Andes-Amazon transition (Cazorla et al., 2022; Condom et al., 2020; Falco et al., 2019; Fassoni-Andrade et al., 2021; Gibson et al., 2019).

Our study aims to validate RCMs in their ability to accurately simulate the spatial distribution, seasonal patterns, and interannual variability of precipitation within the Andes-Amazon transition region. To this end, we employ 30 GCM-RCM simulations, encompassing models within the CORDEX framework and the Eta RCM. In our analysis, we aim to elucidate the primary biases and strengths exhibited these models. Additionally, we delve into a less explored aspect of RCM evaluation, namely the orographic precipitation patterns found within the rainfall hotspots. Lastly, we assist in the selection of suitable GCM-RCM combinations for the Andes-Amazon transition region by ranking the performance of each simulation in the reproduction of various precipitation features.

2. Study Area and Data Sets

2.1. Study Area

Our study centers on the Andean-Amazon transition region, delineated by the coordinates 0°–16°S and 80°–69°W (Figure 1). This region encompasses the Peruvian-Ecuadorian Andean highlands within the Amazon basin, the eastern slopes of the Andes, and the western Amazon lowlands (altitudes below 500 m.a.s.l.).

In this region, two major Andean-Amazonian river basins are present: the Marañón and the Ucayali river basins. The Marañón and the Ucayali rivers are the main northwestern and southern tributaries, respectively, of the Peruvian Amazon River (blue contoured lines in Figure 1). These areas are further explored separately due to their distinct spatio-temporal precipitation patterns, primarily within the Andes-Amazon transition region (Espinoza et al., 2009; Figueroa et al., 2020; W. Lavado-Casimiro & Espinoza, 2014; W. S. Lavado-Casimiro et al., 2013; Valenzuela et al., 2023).

2.2. Reference Precipitation Data Sets

We chose two precipitation gridded data sets as reference data sets to address observational uncertainties. First, we utilized "Rain for Peru and Ecuador" (RAIN4PE version 1), which is a reverse hydrological model derived from multi-source precipitation data sets (Fernández-Palomino et al., 2022). Second, we employed the "Climate Hazards Group InfraRed Precipitation with Station data" (CHIRPS 2.0), a product that blends satellite and rain-gauge data (Funk et al., 2015). Monthly timestep data from 1981 to 2005 was used to match "historical" RCM simulations.

It is worth noting that RAIN4PE demonstrated superior performance compared to several other precipitation gridded products, including CHIRPS, when compared against rain-gauge data within the Andes-Amazon transition region (Fernández-Palomino et al., 2022). Furthermore, when employed as a hydrological model input, RAIN4PE was the only precipitation data set to achieve water budget balance, significantly enhancing the accuracy of daily streamflow simulations within our study area (Fernández-Palomino et al., 2022).

Given that the diagnosis of water budget coherence appears as an effective method to assess the quality of precipitation gridded data sets (Fassoni-Andrade et al., 2021), we are confident enough to select RAIN4PE as the main reference data set and CHIRPS as a secondary reference data set.

To evaluate the spatial variability of orographic rainfall across the Andes-Amazon transition region, we employed the GTOPO30 elevation data set (Earth Resources Observation and Science (EROS) Center, 2018). This data set offers a horizontal grid resolution of 30 arc seconds, which is approximately equivalent to 1 km. To match the precipitation gridded data sets' horizontal grid resolution, a conservative remapping was performed.

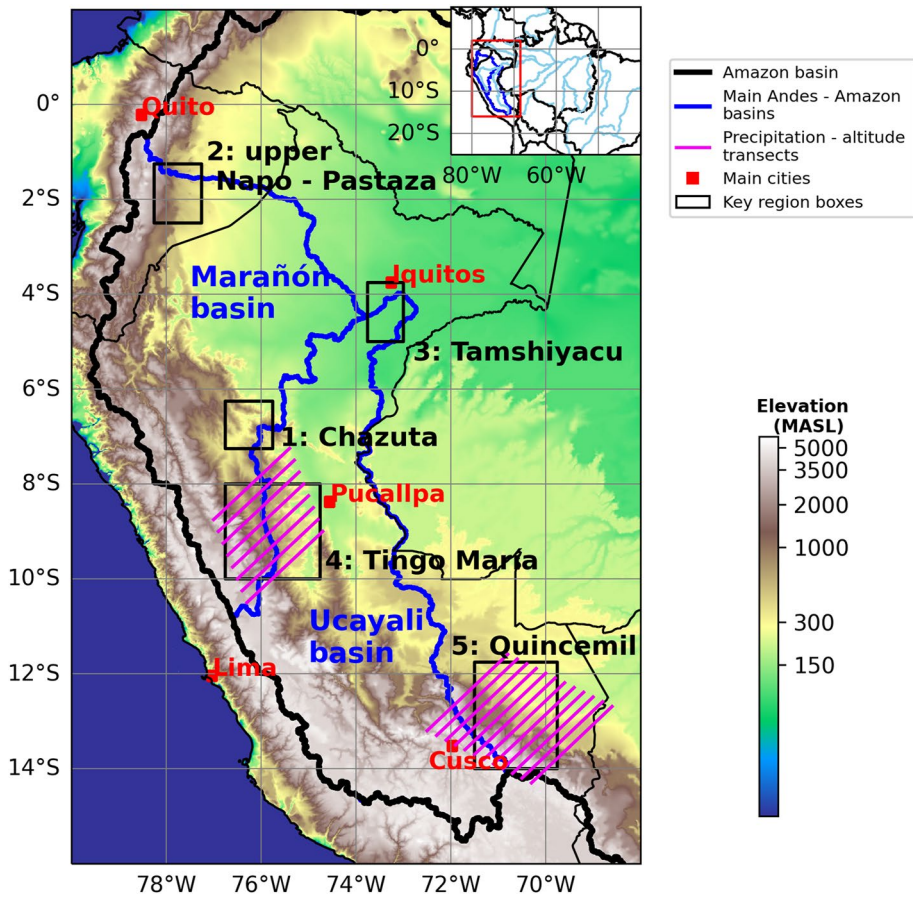

Figure 1. The Andes-Amazon basin with topography (GTOPO30) depicted in shades. Boxes 1, 2, 3, 4, and 5 represent Chazuta, upper Napo-Pastaza, Tamshiyacu, Tingo María, and Quincemil regions. Purple hatching represents the transects followed to explore the precipitation-topography variability over two precipitation hotspots (i.e., Tingo María and Quincemil, see Section 3.3).

2.3. RCM Simulations

We obtained monthly mean daily (mm/day) precipitation data from 30 "historical" RCM simulations for the South American domain. This data was sourced from the ESGF site (esgf-data.dkrz.de/search/esgf-dkrz/) at varying horizontal spatial resolutions: 0.5°, 0.44°, 0.22°, and 0.20°, hereinafter referred to as S50, S44, S22, and S20, respectively. The analysis period spans from 1981 to 2005.

These simulations were conducted by five RCMs within the CORDEX-SAM framework. These models are: RegCM v4.7, REMO2015, RegCM v4.3, WRF, and RCA4, denoted as RC47, REMO, RC43, WRF, and RCA, respectively. In addition, we incorporated three complementary simulations that were performed using the Eta model, as described by Chou et al. (2014). Terrain elevation data from each RCM was also collected. Table 1 further summarizes the details of GCM-RCM simulations (single realizations) used in this study. Detailed information about the model physical setup for each RCM can be found in Table A1 in "Description and user guide of the worldwide CORDEX C3S data set assessing potential conflicts due to overlaps" (available at https://confluence.ecmwf.int/display/CKB/CORDEX%3A+Regional+climate+projections).

3. Methods

The evaluation of RCMs was focused on the precipitation climatology, seasonal cycles, and interannual variability across several regions and subregions (Figure 2). We performed a bilinear interpolation of precipitation to a 0.25° × 0.25° common grid size to compute the performance of the models within the reference products. In addition, analyses considered the construction of RCM ensembles, which lets us cluster the simulations into their

Journal of Geophysical Research: Atmospheres

10.1029/2023JD038618

Table 1
Summary of the Regional Climate Model (RCM) Simulations Used in This Study, Showing the Available Global Climate Model (GCM)-RCM Combinations Used Throughout This Study, Spatial Resolutions of RCM Output, and the References of RCMs and Driving GCMs

	RCM and available resolution						
Driving GCM	RCA4	RegCM4.3	RegCM4.7	WRF341Iv2	REMO2015	Eta v1	GCM reference
CanESM2	Both S44 and S50	–	–	S44	–	S20	von Salzen et al. (2013)
IPSL-CM5A-MR	Only S44	–	–	–	–	–	Dufresne et al. (2013)
CNRM-CM5	Both S44 and S50	–	–	–	–	–	Voldoire et al. (2013)
CSIRO Mk3.6	Both S44 and S50	–	–	–	–	–	Rotstayn et al. (2009)
EC-EARTH	Both S44 and S50	–	–	–	–	–	Hazeleger et al. (2010)
HadGEM2-ES	Only S50	S44	S22	–	S22	S20	Collins et al. (2011)
MIROC5	Both S44 and S50	–	–	–	–	S20	Watanabe et al. (2010)
MPI-ESM-LR	Both S44 and S50	–	S22	–	S22	–	Zanchettin et al. (2013)
NorESM1-M	Both S44 and S50	–	S22	–	S22	–	Bentsen et al. (2013)
GFDL-ESM2M	Both S44 and S50	S44	–	–	–	–	Dunne et al. (2012)
RCM reference	Samuelsson et al. (2011, 2015)	Giorgi et al. (2012)	Giorgi et al. (2012)	Skamarock et al. (2008)	Jacob et al. (2012)	Mesinger et al. (2012)	

Note. The dashed lines mean that no GCM-RCM combination is available. Spatial resolutions of the RCM simulations used in this study, namely $0.2° \times 0.2°$, $0.22° \times 0.22°$, $0.44° \times 0.44°$, and $0.5° \times 0.5°$, are represented by S20, S22, S44, and S50, respectively. The red characters within the GCM and RCM names are used as acronyms throughout the text (e.g., HadG for HadGEM2-ES and RC47 for RegCM4.7).

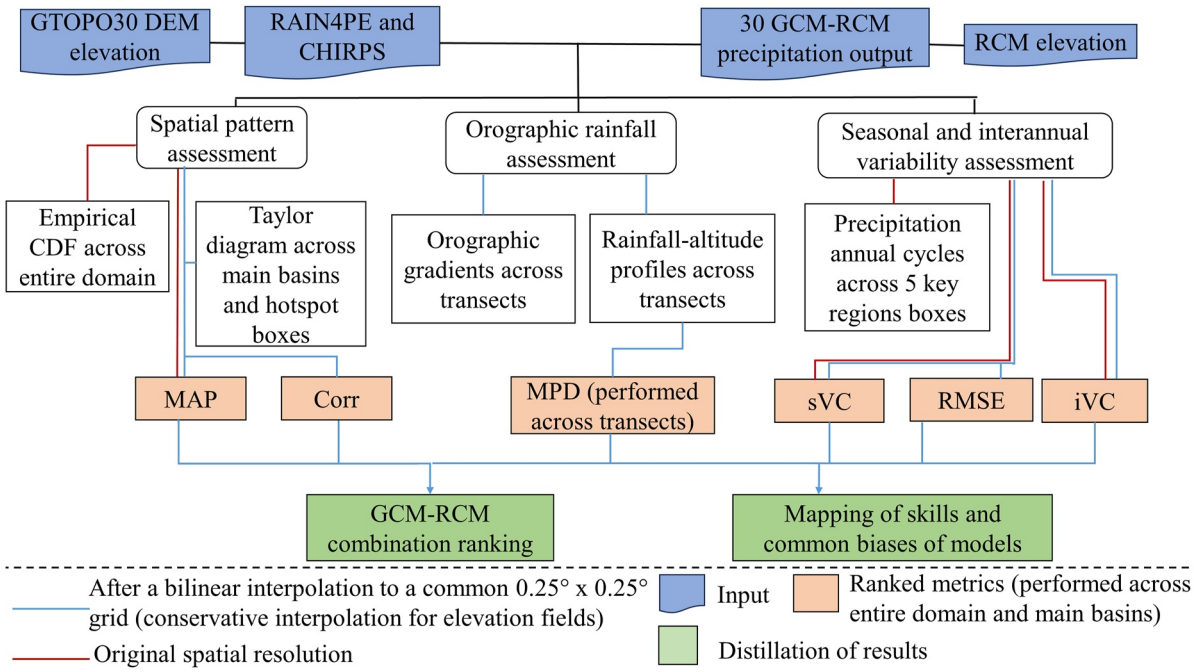

Figure 2. Flowchart of the evaluation process performed in this study. Overall precipitation and equivalent elevation input for the assessment process are marked by blue shapes. Ranked metrics and their visualizations are represented by orange quadrangles. Distillation and summarization of results are represented by green quadrangles. Red lines (blue) represent processes and visualizations that are performed at original grid-size (interpolated grid-size to 0.25° × 0.25°).

downscaling RCM and correspondent spatial resolution. No post-processing, such as bias correction or statistical downscaling, has been applied to the RCM simulations as the purpose of this study is model evaluation.

3.1. Spatial Pattern Assessment

The Taylor diagram (Taylor, 2001) was utilized to assess the skill of the spatial pattern of mean annual precipitation (MAP) simulated by the RCMs in comparison to a specific gridded precipitation data set. The visualization of the Taylor diagram involves three key metrics: Pearson's correlation coefficient (Corr), normalized standard deviation, and normalized root mean square error (RMSE). Normalization is achieved by dividing the standard deviation by the reference standard deviation. Normalized RMSE is obtained by applying a law of cosines-like relationship to the correlation and the normalized standard deviation, as described by Taylor (2001). The reader is referred to Taylor (2001) for more in-depth information on the formulation of these metrics and the underlying technique.

Additionally, the assessment derived from the Taylor diagram was further complemented by employing empirical cumulative density functions (CDFs), which were applied to the mean annual values of each grid cell within the study area.

3.2. Orographic Precipitation Relations Over the Andes-Amazon Transition Region

We performed two precipitation-topography profile analyses (purple hatching in Figure 1) within two distinct rainfall hotspot regions. For each hotspot, a minimum of eight transects were designed to follow a trajectory commencing from the windward side of the mountains and concluding at the eastern Andean summits. To ensure clarity and prevent visual clutter in the figures, we selected the most effective combinations of S20 and S22 RCMs based of their performance as depicted in the Taylor diagrams across both rainfall hotspot regions.

Within these hotspot regions, a linear relationship between elevation and precipitation is not readily discernible; instead, precipitation tends to peak at altitudes ranging from 1,000 to 1,500 m.a.s.l., as observed in prior studies (Chavez & Takahashi, 2017; Espinoza et al., 2015, 2009), Consequently, we calculated orographic gradients, which are defined as the quotient between differences in precipitation rates at two distinct locations and their

Table 2
Summary of the Statistics Used to Rank Regional Climate Model (RCM) Performances

Property	Variable	Calculated as	Error
Spatial pattern	MAP	The annual mean of each grid cell	$\lvert MAP_{ref} - MAP_{rcm} \rvert$
	Corr	Spatial correlation coefficient between MAP_{rcm} and MAP_{ref}	$1 - Corr_{rcm}$
Orographic rainfall	MPD across Quincemil and Tingo María profiles	The average profile of the precipitation and topography transects in references and simulations	$\lvert P_{ref} - P_{rcm} \rvert$ across mean profile
Seasonal variability	sVC	The coefficient of variation between monthly means ($m = 1, 2, \ldots, 12$) of each grid cell	$\lvert sVC_{ref} - sVC_{rcm} \rvert$
	RMSE	The average of monthly mean root mean square error (RMSE) between references and simulations	$\left(\frac{1}{12}\right) \sum_{m=1,2\ldots}^{12} RMSE_{rcm,m}$
Interannual variability	iVC	The coefficient of variation between 12-month-windowed moving averages of monthly precipitation of each grid cell	$\lvert iVC_{ref} - iVC_{rcm} \rvert$

corresponding differences in altitude. These calculations were carried out along two altitudinal sections for each transect, distributed across the two rainfall hotspots under investigation (see Figure 1). These sections were split by the altitude at which the precipitation maximum is located. Thus, the lower section is bounded by the minimum precipitation in lowlands and the precipitation maximum, and the upper section extends from the precipitation maximum to the summits.

3.3. Seasonal and Interannual Timescales Assessment

The analysis of annual cycle regimes was concentrated on five distinct regions within the Andes-Amazon transition region area. These regions include Chazuta, upper Napo-Pastaza, Tamshiyacu, Tingo María, and Quincemil, with their boundaries demarcated by the outlined boxes in Figure 1.

Following Espinoza et al. (2009), seasonal and interannual rainfall variability over the Andes-Amazon basin were evaluated using the seasonal coefficient of variation (sVC) and the interannual coefficient of variation (iVC), respectively. The sVC was computed by determining the coefficient of variation for the monthly mean precipitation values within each grid cell. To calculate the iVC, we initially applied a 12-month moving average with a sliding temporal window to emphasize the annual variability. Subsequently, we calculated the coefficient of variation for the smoothed time-series data, resulting in the iVC (1981–2005) values for each grid cell.

Additionally, we computed the monthly mean RMSE for each grid cell's monthly mean precipitation climatology, employing RAIN4PE as the reference data set.

3.4. Metrics to Rank the RCM Performances

Inspired by Mascaro et al. (2018), we computed an error metric for each of the seven metrics defined above (Table 2). Error metrics were developed for MAP and spatial correlation to evaluate the spatial distribution. Mean precipitation profile differences (MPD) between RCMs and the reference data set were used to assess the orographic rainfall within the precipitation hotspots. In addition, error metrics for sVC and RMSE (iVC) were constructed to evaluate seasonal (interannual) variability.

Subsequently, we assigned a ranking to each model based on the performance according to each error metric, with lower rankings indicating superior RCM performance. Additional details regarding the formulation of these error metrics can be found in Supporting Information S1.

4. Results

4.1. Spatial Pattern and Annual Cycles of Rainfall Simulated by RCMs

We validate RCM simulations based on the patterns represented by RAIN4PE and CHIRPS precipitation data sets. Both reference data sets exhibit a north-to-south gradient over the Amazonian lowlands, with a maximum over the Equator above 6 mm/d and at the Ecuadorian eastern Andean slopes, with maximums of 10–14 mm/d

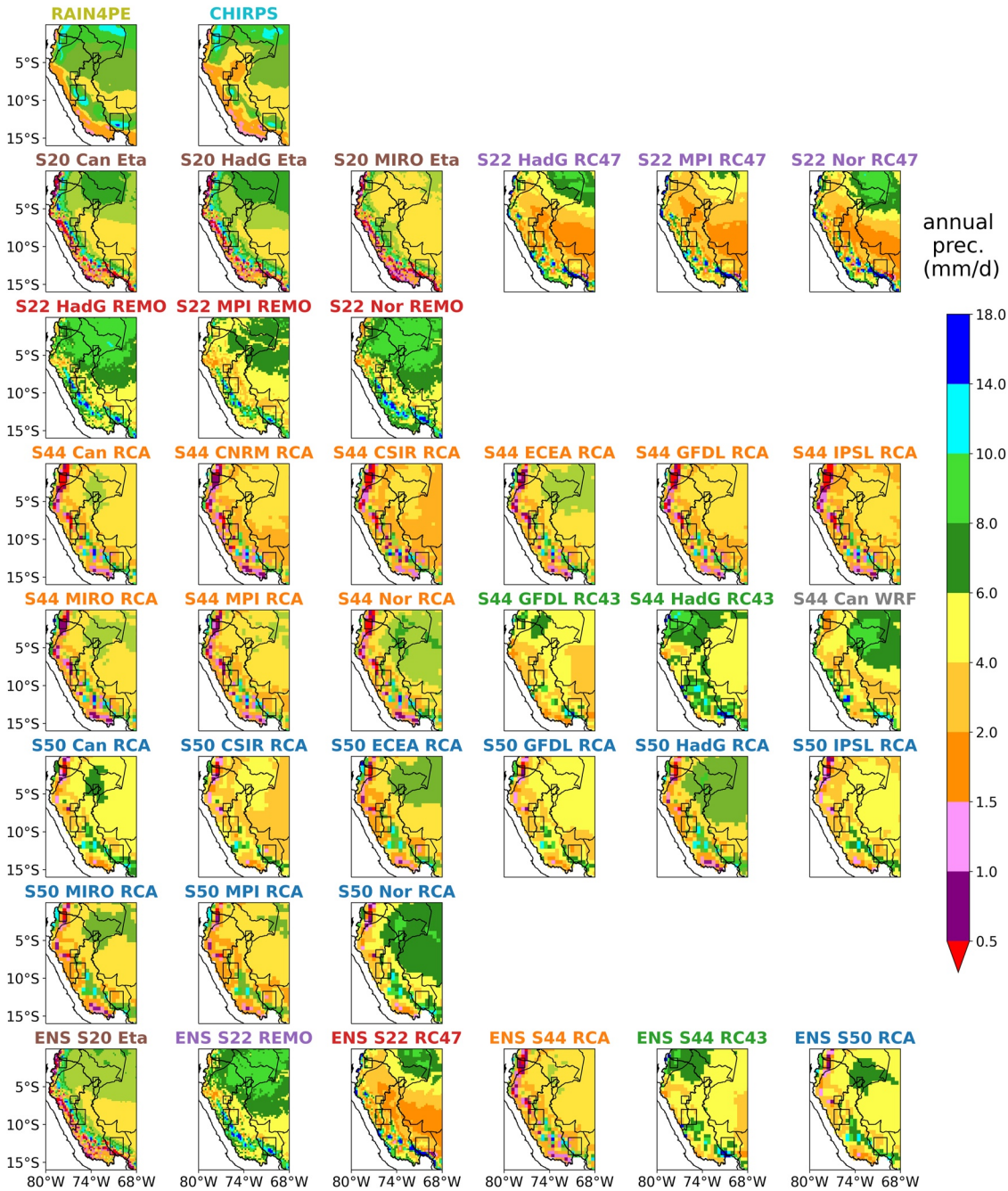

Figure 3. Daily mean precipitation between 1981 and 2005 for the western Amazon basin for the (first row) precipitation gridded data sets, (second and third row) S20 and S22 horizontal resolution regional climate model (RCM) output, (fourth and fifth row) S44 horizontal resolution RCM output, (sixth and seventh row) S50 horizontal resolution RCM output, and (eighth row) RCM ensemble means. Same colors on the names represent simulations belonging to the same RCM, and this color code will be used throughout the paper.

(first row of Figure 3). Additionally, both products depict a continuous rainfall hotspot along the eastern flank of the Peruvian Andes, featuring two rainfall hotspot maximums above 10 mm/d over Quincemil (12.5°S, 70.5°W) and Tingo María (9°S, 75.5°W). Furthermore, at the Andean highlands (>4,000 m.a.sl., see Figure 1), the data sets consistently indicate low precipitation rates, typically below 4 mm/d.

The three S20 Eta simulations successfully capture the north-to-south precipitation gradient, and represent a relatively narrow, continuous rainfall hotspot region, albeit without clear maximum centers (Figure 3, second row). However, Eta simulations exhibit significant spatial variability in the Andean highlands, with certain grid

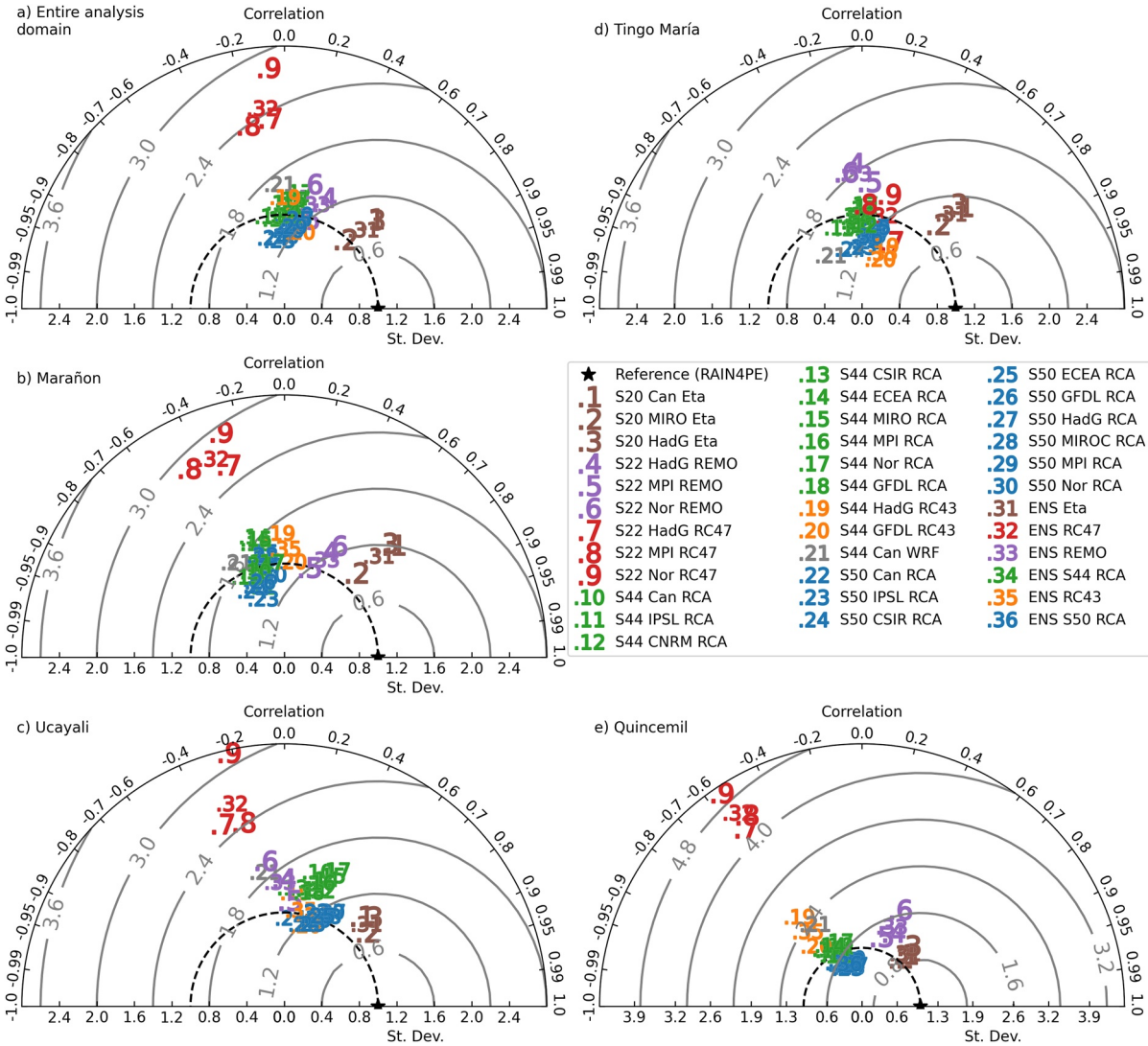

Figure 4. Taylor diagram showing the 30 global climate model-regional climate model (GCM-RCM) combinations and 6 RCM ensembles over (a) the entire domain (see Figure 1), (b) Marañón basin, (c) Ucayali basin, (d) Tingo María box, and (e) Quincemil box (see Figure 1). Same colors represent simulations belonging to the same RCM. RAIN4PE was selected as the reference data set. RAIN4PE and GCM-RCM combinations have been interpolated to a common 0.25° spatial grid resolution. The black star represents the reference values where the spatial correlation and the normalized standard deviation is equal to 1. Dashed black semicircle is located where normalized standard deviation is equal to 1. The radial distance from the black star quantifies the RMSE normalized by the reference standard deviation. The radial distance and the azimuthal position from the origin quantify the normalized standard deviation and the spatial correlation, respectively.

cells displaying dry conditions (below 1 mm/d) and other receiving higher annual precipitation (ranging from 6 to 10 mm/d). Notably, the overestimations are more pronounced in the southern part of the Andean highlands (13–15°S), with the most significant biases occurring during the summer months (not shown).

Furthermore, the Taylor diagram in Figure 4 reveals that Eta performs most effectively in replicating spatial patterns across basins and precipitation hotspots, as seen by correlations ranging from 0.3 to 0.6 when compared to RAIN4PE.

S22 REMO simulations tend to exhibit excessive precipitation over the eastern Andean summits. These simulations shift the orographic rainfall maximum westward, moving it upward along the slopes and resulting in excessive precipitation over the Andean highlands (>4,000 m.a.s.l.) south of 10°S. Some grids represent precipitation rates of approximately 4–8 mm/d in stark contrast to the observed 1–3.5 mm/d, leading to overestimations ranging from 100% to 800%.

Similarly, the S22 RC47 simulations also manifest an overproduction of precipitation over the summits, particularly in the vicinity of the Quincemil hotspot, where precipitation levels reach 50 mm/d. This corresponds to a

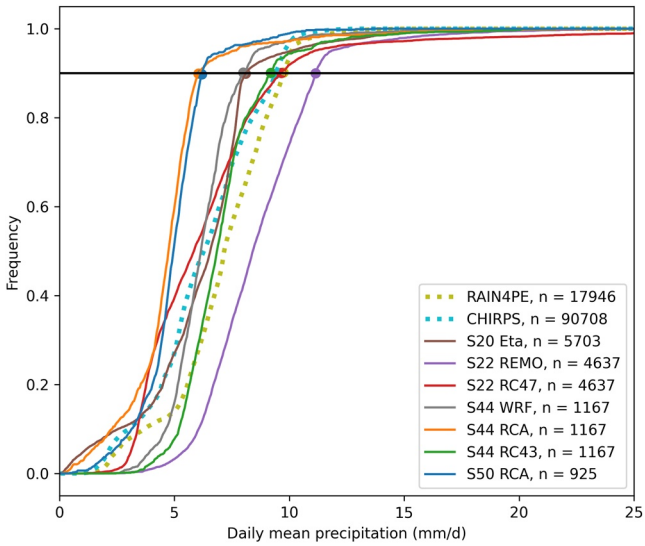

Figure 5. Empirical cumulative distribution function of daily mean precipitation (mm/d) over the entire domain for RAIN4PE, CHIRPS, and RCM ensembles. A black line is drawn at the non-exceedance probability of 90%.

25-fold overestimation in certain locations. Additionally, these simulations depict a drier Amazon region south of 5°S, with precipitation rates ranging from 1.5 to 2 mm/d, in comparison to the observed 2–6 mm/d, as well as a drier eastern slope (1.5–4 mm/d compared to the observed 8–13 mm/d). Furthermore, these simulations rank the lowest in performance according to the Taylor diagram, characterized by the strongest spatial variances (2.2–4.3) and negative to near-zero anticorrelations (ranging from −0.6 to 0.1), particularly at the hotspots.

Regarding the S44 and S50 resolutions, RCA simulations severely underestimate rainfall over the eastern Andean slopes between 0 and 6°S, with the Ecuadorian region experiencing particularly significant underestimations (approximately 0.5–1.5 mm/d compared to the observed 6–11 mm/d). In contrast, the RC43 simulations offer a more accurate representation of this region.

The RCA simulations, when driven by ECEA, MIRO, Nor, and HadG, successfully capture the latitudinal gradient of rainfall from the Equator to 16°S, producing a spatial maximum over the equatorial Amazon lowlands. Moreover, these GCM-RCM combinations partially replicate the orographic rainfall pattern south of 10°S in the precipitation hotspot region, although they exhibit some wet biases over the mountain summits.

When dividing the entire domain into the Marañón and Ucayali basins (Figures 4b and 4c), it becomes apparent that the S44–S50 RCA simulations generally perform better in the latter basin, as quantified by the higher correlations (−0.4 to 0 compared to 0 to 0.25). This discrepancy may be attributed to the substantial underestimation of precipitation over the Ecuadorian eastern slopes by these models (approximately 0.5–1.5 mm/d compared to 6–11 mm/d).

Overall, across all simulations ranging from S20 to S50, wet biases over the Andes are stronger during the summer season (not shown), being a recurrent bias in both GCM and RCM simulations at the Andean cordillera (e.g., Falco et al., 2019; Ortega et al., 2021).

The spatial mean of the RCM ensembles (last row of Figure 3) shows that while the highest resolution model (S20 Eta) tends to yield the best results, increasing the spatial resolution of available RCMs from S50 to S20 does not consistently improve precipitation patterns in the Andes-Amazon transition region. Notably, lower performance exhibited by the S22 RC47 model across different basins and precipitation hotspots is the strongest argument in support of this observation. S22 RC47 performance degrades in comparison to S44 RC43 as the former simulates drier Amazonian lowlands south of 5°S and greatly overestimates precipitation at the summits, with certain grid points reaching precipitation rates as high as 50 mm/d. However, besides spatial resolution, RC47 and RC43 models also differ in their physical setup, particularly regarding their convection and land surface parameterization schemes (see Section 2.3). While the S20 Eta model excels in reproducing precipitation pattern in the hotspots, the S22 REMO model still maintains overestimations over the eastern Andean flank slopes and summits (around 8–20 mm/d; Figure 6). The REMO model is the second-best model at the Marañón basin and Quincemil with the best correlations being around 0.3, but does poorly regarding spatial pattern correlation over the Ucayali basin and the Tingo María hotspot.

The resulting empirical CDF summarizes the wide ranges of the simulated spatial variabilities by the RCM ensembles, as seen in Figure 5. The overestimation of precipitation by the REMO model is evident along all percentiles, and its 90th percentile is about 1.4 mm/d higher than RAIN4PE and CHIRPS. Similarly, the RC47 model demonstrates overestimation at percentiles higher than 96, reaching its maximum at around 55 mm/d (not shown in the figure *x*-axis). This model also underestimates precipitation as shown until percentile 50, as a result of underestimation on Amazonian lowlands south of 5°S. The RCA model tends to underestimate precipitation due to strong dry biases over most of the study area along all percentiles. The Eta CDF resembles more the CHIRPS CDF, although it seems to slightly underestimate 35% of its pixels, and its percentile 90 is underestimated by 1.6 mm/d. RC43 CDF overestimates precipitation up to its eighteenth percentile, which can be attributed to the absence of annual precipitation rates below 2 mm/d in the study area.

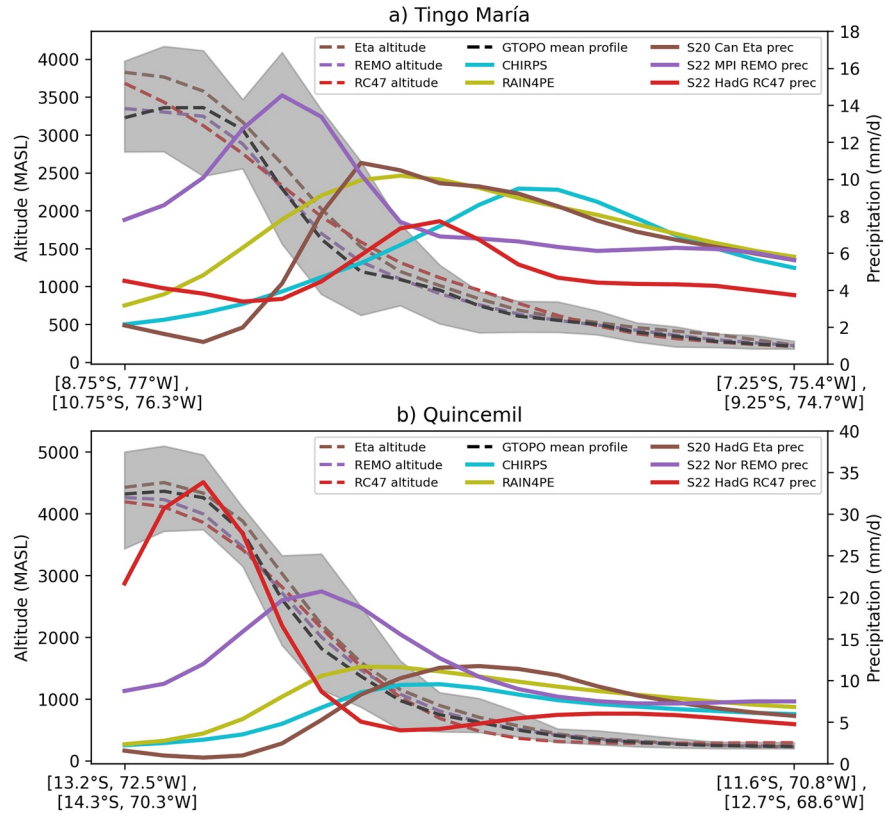

Figure 6. Mean profiles of topographical height (dashed lines) and daily mean precipitation (solid lines) of CHIRPS, RAIN4PE, and selected S20 and S22 global climate model-regional climate model (GCM-RCM) combinations through the transects constructed across (a) Tingo María and (b) Quincemil (over region 4 and 5, respectively, see Figure 1). Gray shading represents maximum and minimum altitude across transects by GTOPO30. Single S20 and S22 GCM-RCM combinations over Tingo María and Quincemil are selected on the basis of the "best" spatial pattern member within the RCM ensemble, as seen in Figure 3. Transects follow a windward-summit orientation (from right to left on this figure).

4.2. Orographic Rainfall

Both RAIN4PE and CHIRPS show heterogeneous representations of rainfall across both hotspots, as shown in Figure 6. Specifically, over Tingo María, RAIN4PE (CHIRPS) locates a precipitation maximum at 1,150 (600) m.a.s.l. Similarly, in Quincemil, RAIN4PE (CHIRPS) places the maximum at 1,300 (1,000) m.a.s.l. It is noteworthy that RAIN4PE and CHIRPS also exhibit varying precipitation quantities within the regions spanning 1,500–3,000 m.a.s.l., with RAIN4PE producing approximately twice the precipitation rates compared to CHIRPS within this altitude range.

Regarding selected S20 and S22 RCM simulations, the Eta RCM closely aligns with the quantities and altitudes of the precipitation maximum observed in both profiles when compared to gridded data sets. However, it is important to note that precipitation rates to the west of this maximum decrease rapidly upslope across the Tingo María and Quincemil profiles.

In Quincemil, RC47 tends to significantly underestimate precipitation rates along the slopes (500–1,500 m.a.s.l) with values around 3.5 mm/d, while the observed maximum (10–12 mm/d) is located between 1,000 and 1,500 m.a.s.l. This model also produces an overestimated maximum (mean of 35 mm/d) at an altitude of 4,100 m.a.s.l, whereas the gridded products indicate precipitation rates below 5 mm/d at this altitude.

It is worth noting that both the best and the worst performances are found with the highest resolution models (S20 Eta, S22 REMO, and S22 RC47). Excessive precipitation orographic gradients further illustrate that S22 spatial resolution RCMs may have stronger biases than the S44 and S50 RCMs across both precipitation hotspots (Figure 7). High orographic gradients between minimum in lowlands and precipitation maximum in the Tingo María hotspot in CHIRPS and RAIN4PE may be a consequence of the relatively low altitude of the precipitation maximum, thereby diminishing their altitudinal differences. Some simulations'

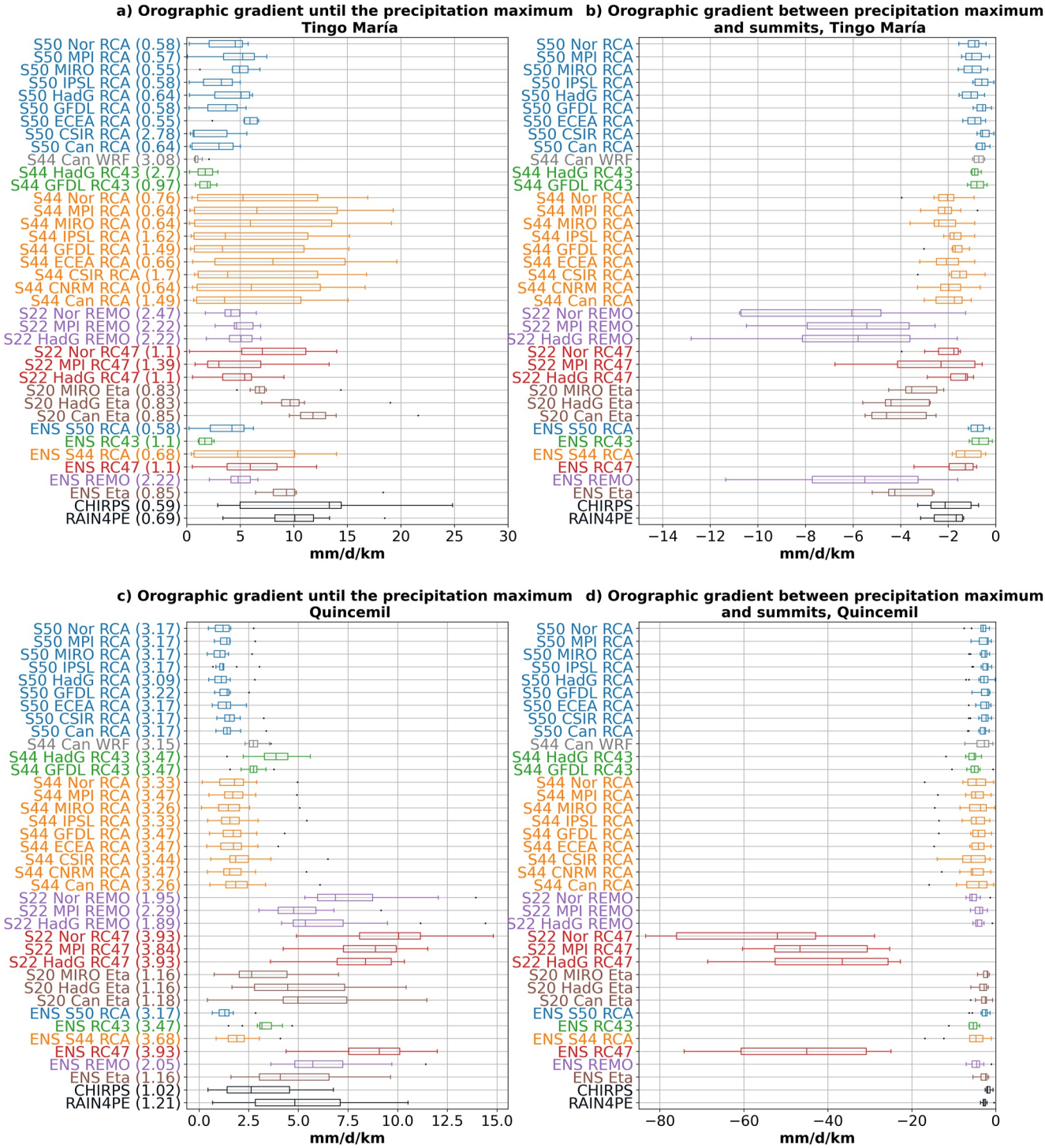

Figure 7. Boxplots of orographic gradients (calculated as the quotient between differences in precipitation rates at two locations and their corresponding altitudes) across transects over both precipitation hotspots (see Figure 1). Orographic gradients in (a–c) were calculated in the "lower" section of each transect (i.e., between minimum at lowlands and the precipitation maximum). Orographic gradients in (b–d) were calculated in the "upper" section of each transect (i.e., between precipitation maximum and the summits). Numbers in parenthesis in (a–c) represent the median altitude of maximum precipitation (in km) across transects for each simulation/ensemble.

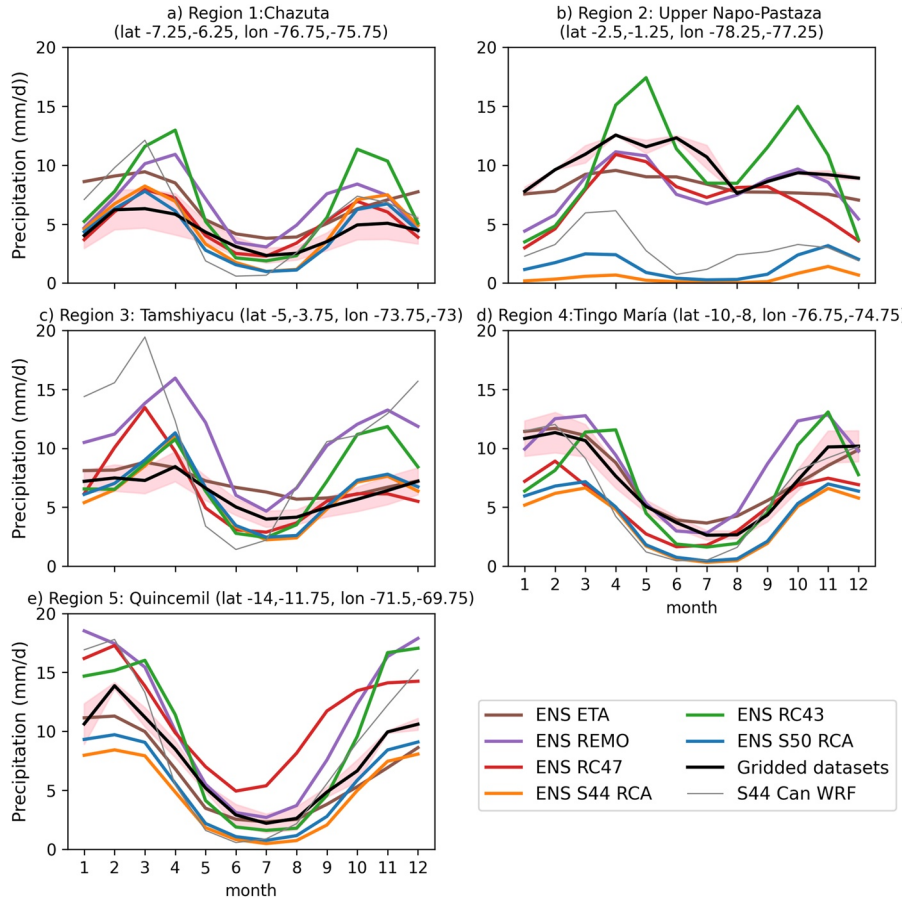

Figure 8. Annual regimes of precipitation mean between 1981 and 2005 for the five boxes defined in Figure 1. The thick black line and shading around it represents the average annual cycle and spread among RAIN4PE and CHIRPS, respectively. Spread characterizes the maximum and minimum monthly climatologies between RAIN4PE and CHIRPS.

orographic gradients may appear closer to the observed values due to compensations caused by increases of altitudinal differences, as a consequence of the overestimation of the altitudes of precipitation maximums (Figures 7a–7c).

Focusing in the highest resolution RCMs, the Eta model simulations are closer in representing the altitude of the spatial maximum in both hotspots (between 590 and 1,210 m.a.s.l.). In contrast, REMO and RC47 tend to simulate the spatial maximum at higher altitudes in comparison to the observed data. These model differences have an important effect masking the results of the orographic gradient, which would otherwise be higher if maximum precipitation altitudes were closer to the observations. However, in the case of the Quincemil hotspot, RC47 notably stands out with the most substantial orographic gradient until the precipitation maximum as a result of its prominent wet bias (around 50 mm/d) around 3,900 m.a.s.l (see Figure 6). Furthermore, REMO and RC47 simulations exhibit the most prominent negative orographic gradients between the precipitation maximum and the summits in Tingo María and Quincemil, respectively. In the Eta RCM simulations, the orographic gradients between the precipitation maximum and the summits are roughly twice the magnitude of the observed values, possibly due to strong underestimations occurring after the maximum is reached over both hotspots. However, it is more consistent with RAIN4PE and CHIRPS over Quincemil.

4.3. Seasonal Variability

RCM simulations across the Andes-Amazon transition region successfully capture the overall seasonal fluctuations. However, some RCMs tend to overestimate precipitation mostly during the rainy seasons, especially in the equatorial-most boxes (Figures 8a–8c). Among the analyzed boxes, certain RCMs can effectively represent the bimodal cycle observed in these regions (Laraque et al., 2007; Segura et al., 2019).

For the Upper Napo-Pastaza and Tamshiyacu boxes, the Eta ensemble displays a relatively uniform pattern throughout the year. However, it is worth noting that individual simulations within this ensemble exhibit significant variability in their seasonal cycles (not shown). In contrast, RC43 and REMO consistently produce overestimations of approximately 100% during the peak rainy seasons in February–April and October–November.

In the case of the Upper Napo-Pastaza box (Figure 8c), both the RCA ensembles and the WRF simulation exhibit a dry bias (not lower than 70%) throughout the year. Notably, these models simulate almost no precipitation during June–August, whereas RAIN4PE and CHIRPS data indicate an average rainfall rate of around 10 mm/d during that period.

In the southernmost boxes of Tingo María and Quincemil (Figures 8d and 8e), RCMs generally exhibit a higher level of agreement in terms of the shape and quantities of the seasonal cycle, albeit with some biases present in specific ensembles. For instance, in Tingo María, the S44 RC43 ensemble and both S44 and S50 RCA ensembles erroneously simulate a bimodal cycle. Specifically, RC43 overestimates rainfall during April and September–November compared to gridded data sets. Furthermore, the S22 REMO ensemble overestimates precipitation during August–November in comparison to RAIN4PE data.

In Quincemil, all simulated and observed seasonal cycles show an unimodal regime. Nevertheless, the S44 RC43 and S22 REMO ensembles overestimate precipitation during October–April and September–April, respectively. S22 RC47 also overestimates precipitation during August–March, primarily due to excessive quantities simulated at altitudes above 2,000 m.a.s.l. Moreover, the S44 and S50 RCA ensembles tend to underestimate precipitation throughout the year.

The spatial pattern of seasonal variability is illustrated by sVC maps in Figure 9. Notably, certain features, such as the low seasonality observed over the equatorial western Amazon and its subsequent increase south of 6°S are most accurately captured by the Eta RCM. Furthermore, the Eta RCM adequately reproduces the sVC pattern over the Andean highlands.

In contrast, REMO and RC47 models exhibit higher seasonal variability over the equatorial Amazon (0.2–0.4) while simulating lower seasonal variability in the Andean highlands, resulting in sVC values below 0.5. In addition, RC43, RCA, and WRF models simulate an excessive degree of seasonal variability over the Amazon lowlands south of 5°S, with sVC values exceeding 0.7.

4.4. Interannual Variability

Figure 10 shows the iVC of precipitation gridded data sets and GCM-RCM combinations for the period between 1981 and 2005. Both gridded products consistently identify the Andean highlands as the region with the highest interannual variability. However, there are scattered regions in the Amazonian lowlands north of 7.5°S that exhibit relatively high interannual variability (iVC > 0.15). In addition, RAIN4PE represents lower interannual variability at the Marañón basin than CHIRPS.

None of the GCM-RCM combinations adequately represent the iVC spatial pattern, with a general tendency to underestimate it, particularly over the Amazonian lowlands, where most GCM-RCM combinations show iVC values below 0.1 (Figure 10). Regarding S20 and S22 RCMs, the Eta and RC47 RCMs, and notably MIRO and HadG Eta and Nor RC47, demonstrate a relatively high interannual variability (iVC between 0.2 and 0.5, second row in Figure 10) over the Andean highlands. In contrast, REMO RCM simulates low interannual variability (iVC below 0.1) over the Andean highlands. Almost none of these GCM-RCM combinations simulate significant interannual variability conditions over the Amazonian lowlands north of 7.5°S, which suggests they are unable to reproduce it.

4.5. Final Rankings and Summary of Results

Figure 11 presents the rankings of GCM-RCM combinations based on the assessment of seven spatio-temporal features outlined in Table 2, focusing on precipitation during the 1981–2005 period in the Andes-Amazon transition region, with RAIN4PE serving as the reference. Within these metrics, the Eta RCM excels in the spatial and seasonal aspects, as evident in the first six rows of Figure 11.

The assessment of interannual variability assessment carries out uncertainties due to large spread of iVC, especially in the Amazonian lowlands. However, as seen in Figure 9, no GCM-RCM combinations exhibit significant skill in representing the spatial features of interannual variability, besides some S20 and S22 GCM-RCM combinations at the Andean highlands. The actual iVC error values exhibit minimal differences between models, with

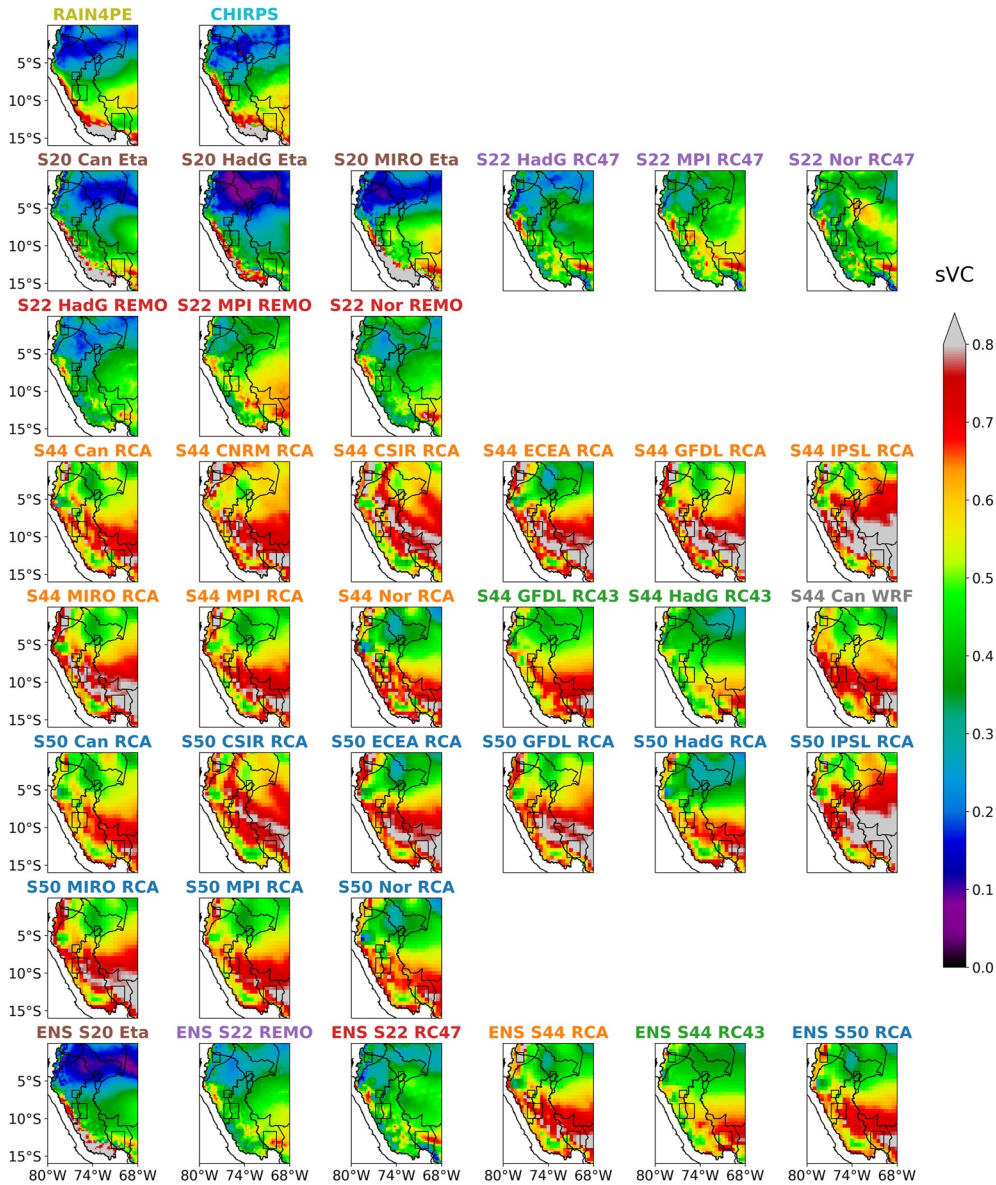

Figure 9. Seasonal coefficient of variation (sVC) calculated from monthly precipitation between 1981 and 2005 for the (first row) precipitation gridded data sets, (second and third row) S20 and S22 horizontal resolution regional climate model (RCM) output, (fourth and fifth row) S44 horizontal resolution RCM output, (sixth and seventh row) S50 horizontal resolution RCM output, and (eighth row) RCM ensembles means.

the best and least ranked models yielding 0.026 and 0.082, respectively, differing by only 0.056 (Figure S4 in Supporting Information S1).

Furthermore, it might be expected that high-resolution simulations (S20 and S22) would outperform low-resolution simulations (S44 and S50). However, S22 RC47 simulations are surpassed by several lower resolution simulations across multiple metrics. Additional analyses are presented using CHIRPS as a reference (Figure S4 in Supporting Information S1). The results prove to be more sensitive over both of the analyzed rainfall hotspots (i.e., Quincemil and Tingo María profiles). Nevertheless, Eta consistently remains as the top-performing model under both reference data sets.

Figure 12 summarizes the main findings in the Andes-Amazon transition region. The spatio-temporal distribution of seasonality is well-represented across the study area, with the Eta RCM performing best in simulating the spatial distribution of seasonality. In the northern Marañón basin, it is crucial to consider the representation

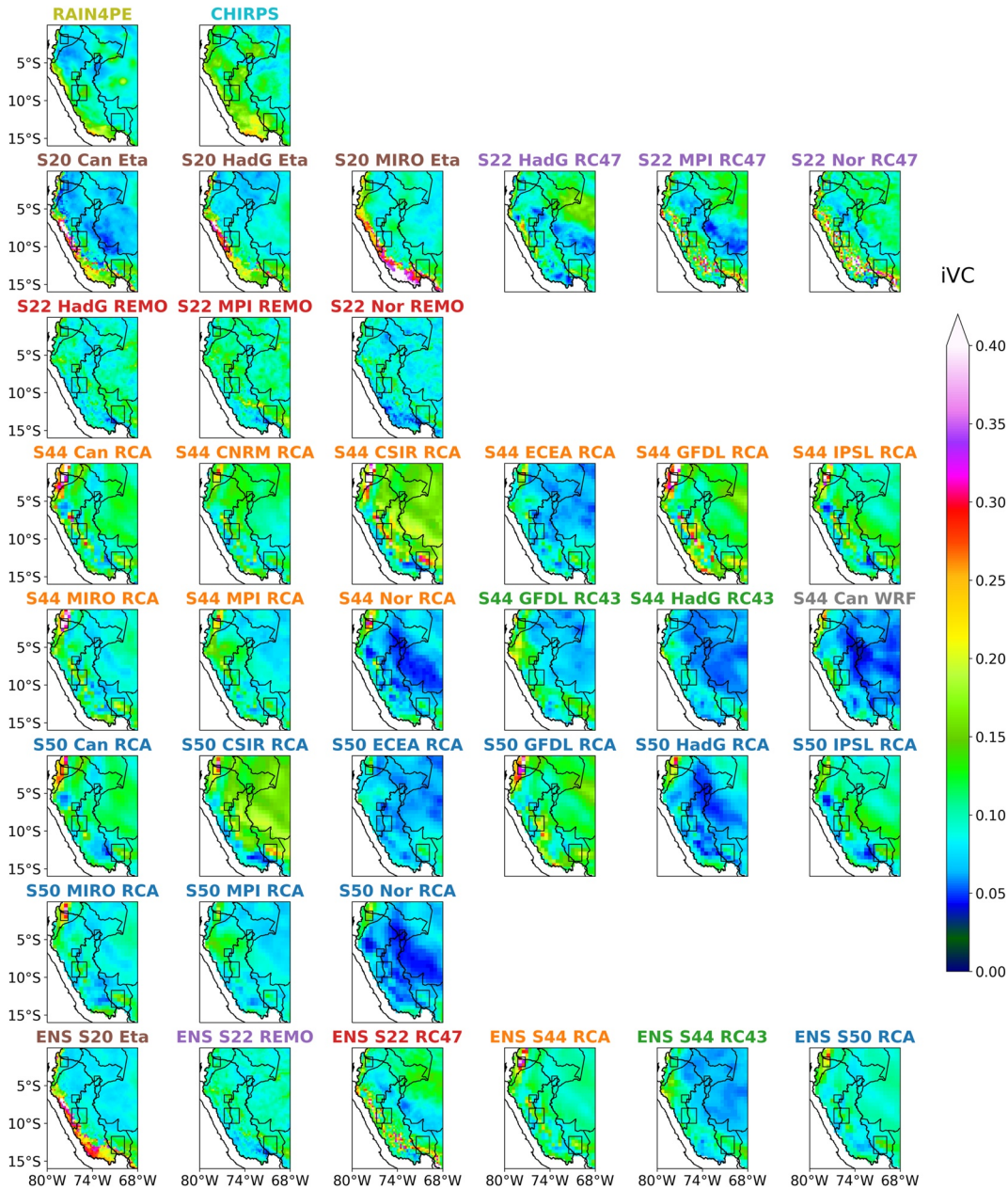

Figure 10. Interannual coefficient of variation (iVC) calculated from mean annual precipitation timeseries between 1981 and 2005 for the (first row) precipitation gridded data sets, (second and third row) S20 and S22 horizontal resolution regional climate model (RCM) output, (fourth and fifth row) S44 horizontal resolution RCM output, (sixth and seventh row) S50 horizontal resolution RCM output, and (eighth row) RCM-averaged iVC.

of rainfall in the equatorial Andes and lowlands. Only the Eta and RC43 models capture the spatial maximum at the eastern flank of the Ecuadorian Andes, with precipitation rates ranging from 10 to 14 mm/d. Some Eta and REMO simulations, particularly those forced by Can and HadG, and by HadG and Nor, respectively, successfully reproduce a continuous equatorial maximum in the lowlands. These simulations exhibit similar precipitation intensity as RAIN4PE and CHIRPS. Moving to the southern Ucayali basin and the rainfall hotspots region, Eta and some S50 RCA simulations effectively depict the spatial extent of rainfall hotspots. Among these models, Eta is the most accurate in representing the altitude of the maximum (1,000–1,500 m.a.sl.).

Regarding biases, in the lowlands and the Andes-Amazon transition region, models tend to exaggerate the annual cycle of precipitation, leading to overestimations during peak months, with RC43 and REMO reaching biases of

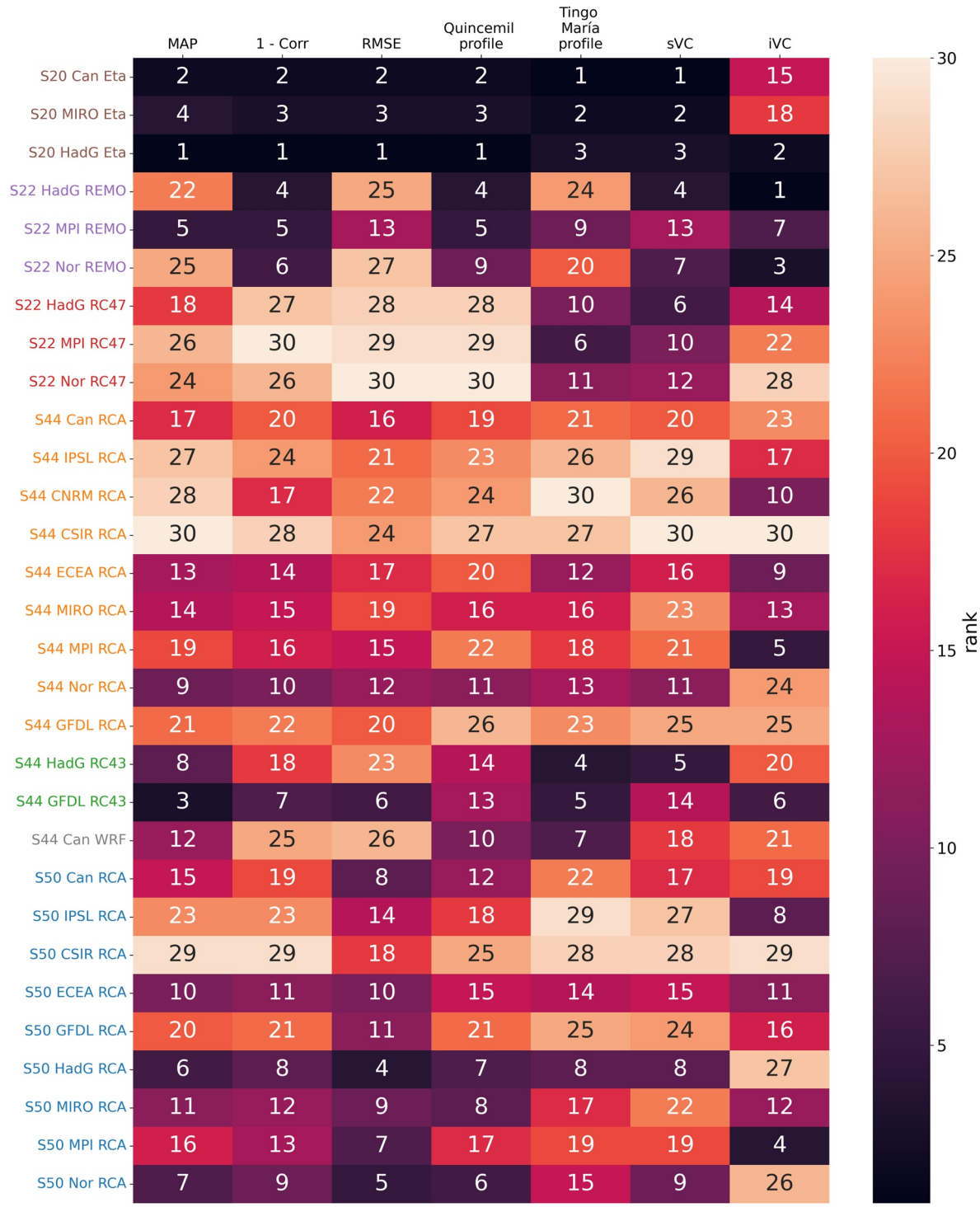

Figure 11. Ranks of the relative error defined in Table 2 for the seven spatio-temporal properties over the western Amazon basin with RAIN4PE used as the reference.

approximately 100% during the rainiest months. On the Andean eastern slopes of Ecuador, S44 WRF and S44 and S50 RCA models underestimate precipitation by approximately 70%–90%. In the southern region, wet biases related to orographic rainfall in the Andean highlands during summer are common among REMO, RCA43, RC47, and, to a lesser extent, Eta. Another noteworthy bias observed is the upslope shift of rainfall hotspots in most models, leading to overestimations over the summits of the eastern Andean flanks. RC47 stands out with

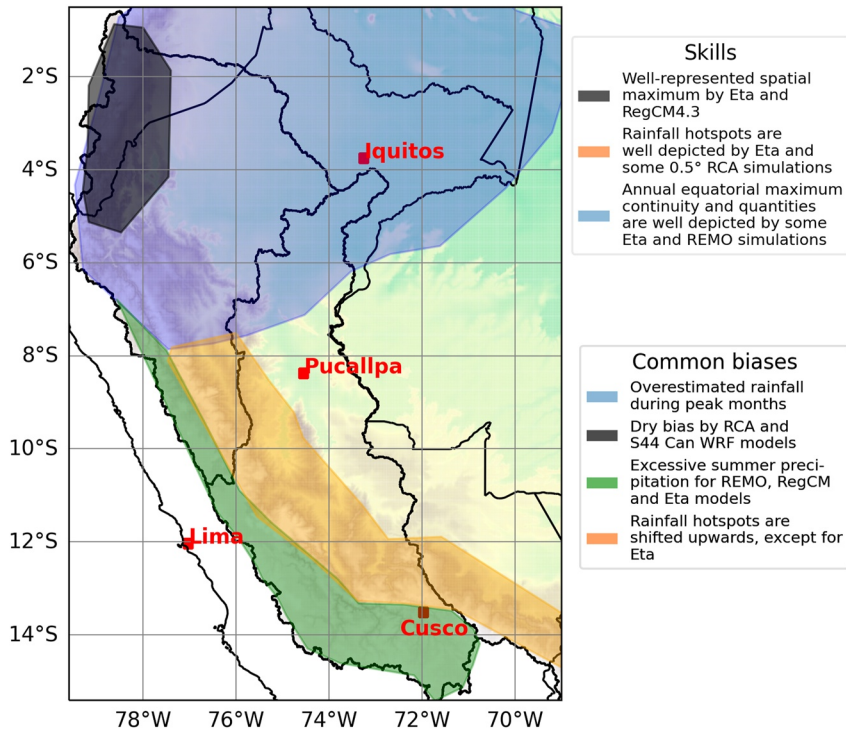

Figure 12. A summary of main findings over the Andes-Amazon transition region. Specific regions are depicted by colors (i.e., the Ecuadorian Amazon slopes are represented by black, the equatorial region by blue, the hotspots region by orange, and the Andean highlands by green).

the most significant wet biases in this region, with certain grids displaying daily precipitation rates in the order of 50 mm/d, which represents an overestimation of approximately 2,500%.

The two latter biases may arise due to the inherent physics of the models and the insufficient spatial resolutions of the simulations to, which hinder their ability to accurately represent rainfall in complex terrain (e.g., Chou et al., 2014; Torma et al., 2015). In addition, another major difference related to the simulation of dynamic processes in mountainous terrain are the vertical coordinates used in the model structure. The Eta model employs eta vertical coordinates, which remain approximately horizontal with respect to mountains (Mesinger et al., 2012). Conversely, the other models utilize either sigma terrain-following vertical coordinates or hybrid vertical coordinates.

5. Discussion

Uncertainties in observational data can significantly influence what is regarded as "skill," particularly in our study area, which is a data-scarce region. We selected RAIN4PE and CHIRPS as reference products based on their performance in grid-to-point comparisons with rain gauges (Fernández-Palomino et al., 2022). Good performances of RAIN4PE as a driver for hydrological modeling in the region further supports its selection as the primary reference product. However, since RAIN4PE is a hydrological model output, caution should be taken as it is still subject to uncertainties related to water cycle components and model input, such as the streamflow, evapotranspiration, precipitation gridded data sets, and the chosen hydrological model structure (Fernández-Palomino et al., 2022).

We found similar results with both RAIN4PE and CHIRPS as reference products (Figures S5–S7 in Supporting Information S1), except for the MPD at the two evaluated precipitation hotspots. Such differences should be expected as the product of observational uncertainties in this region due to scarce monitoring, which limits further calibration of gridded data sets (Condom et al., 2020). Nevertheless, when assessing based on this metric, Eta simulations still holds best performances regardless of precipitation gridded data set used, reinforcing our confidence in its ability in resolving precipitation in this region. Nonetheless, there remains a pressing need

for long-term and comprehensive precipitation monitoring on the eastern slopes of the Andean cordillera. The complex interactions between terrain and regional atmospheric circulation in this area give rise to a wide range of hydroclimatic regimes (Cazorla et al., 2022; Condom et al., 2020). For example, Newell et al. (2022) demonstrated the importance of a network of rain gauges to capture the fine-scale spatiotemporal variability of rainfall in montane cloud forests in the northeastern Andes of Peru. These observations can serve to validate satellite-based and merged precipitation products which can then be utilized as references to properly assess RCM's ability in the reproduction of precipitation patterns over the Amazon's rainiest zone (e.g., Chavez & Takahashi, 2017; Espinoza et al., 2015).

While the highest resolution model (S20 Eta) yields the best results, the impact of increasing RCM resolution from S44–S50 to S20–S22 does not seem to significantly improve the diagnostics of MAP over the rainfall hotspots for all RCMs. In fact, S22 models exhibit worse performance than S44 models for certain criteria. Therefore, aside from horizontal resolution, other model setup characteristics may also affect the model performances (e.g., parameterization, forcing data, vertical levels treatment). Caution should be taken in high-resolution modeling to adequately set-up the model relatively to the climate characteristics of the region of study.

The impact of increasing RCM resolution from S44–S50 to S20–S22 does not appear to markedly affect the diagnostics of MAP over the rainfall hotspots. Previous evaluation studies regarding CORDEX RCMs have suggested spatial resolutions around approximately 12.5 × 12.5 km (not available in CORDEX-SAM) for improved resolution of precipitation due to enhanced topography representation (Lucas-Picher et al., 2017; Mascaro et al., 2018; Prein et al., 2016; Torma et al., 2015). Currently, state-of-art RCMs involve simulations at convection-permitting scales, characterized by spatial resolutions finer than 4 km, enabling the explicit resolution of convection processes without the need for a convective parameterization scheme (Kendon et al., 2021).

At higher spatial resolutions, RCMs in the tropical Andean region significatively improve precipitation features such as the spatial pattern, mesoscale processes linked to the diurnal cycle of convection (Gómez-Ríos et al., 2023; Junquas et al., 2022, 2018; Rosales et al., 2022; Sierra et al., 2022), and the internal structure of mesoscale convective systems and hailstorms (Flores-Rojas et al., 2021; Moya-Alvarez et al., 2019). However, as these spatial resolutions range within the so-called “gray zone” of convection, some local convection processes can be explicitly resolved, while others still require the use of a convection parameterization (Kendon et al., 2021). The interplay between tropical atmospheric circulation regimes and local physio-geographical features further amplifies these uncertainties at very high spatial resolutions (1 km), posing a persistent challenge for the numerical modeling community (e.g., Junquas et al., 2022).

Our results indicate uncertainties in RCM configurations, specifically related to the choice of downscaling model and the physical parameterization schemes. Within set of GCM-RCM combinations considered, these choices appear to exert a more significant influence on the simulation of precipitation, particularly in rainfall hotspots regions.

For example, a common bias highlighted in this study is the dry bias over the eastern Ecuadorian Andes slopes by the RCA model and, specifically, the S44 WRF model. Several WRF-based studies have shown that, under certain parameterizations and higher spatial resolution, precipitation over this region can be either overestimated or improved (e.g., Chimborazo & Vuille, 2021; Junquas et al., 2022; Ochoa et al., 2016). Consequently, the choice of an appropriate convection parameterization scheme becomes crucial in enhancing the reliability of RCM simulations due to better representation of rainfall characteristics.

Many GCM-RCM combinations successfully replicate both unimodal and bimodal annual precipitation patterns in the Andes-Amazon transition region (Espinoza et al., 2009; Segura et al., 2019). However, some combinations tend to overestimate precipitation during peak months at the equatorial-most locations. Additionally, some of them do at the Andean highlands, and the overestimation is stronger during summer. These findings align with the analyses of CMIP5 and CMIP6 GCMs simulations performed by Ortega et al. (2021) and Almazroui et al. (2021), where they also found precipitation overestimations in the tropical Andes, particularly during the rainy seasons. The source of excessive convection at the equatorial-most Andes-Amazon transition region during wet months might be produced mainly by the physics choices of RCMs regarding cumulus convection and land-surface parameterizations, which requires further investigation (Chou et al., 2014).

None of the models is particularly skillful in capturing the interannual variability of rainfall during the period from 1981 to 2005. This challenge may be linked to the complexities associated with simulating related to the

simulation of teleconnection patterns by both GCMs and GCM-driven RCMs (e.g., see Sections 10.4.2. and 10.6 in Doblas-Reyes et al., 2021). Further advancements in this area are imperative, given that precipitation patterns over the Andes-Amazon transition region are significantly influenced by tropical oceans and their interaction with local physio-geographical features (e.g., Arias et al., 2021; Espinoza et al., 2019; Marengo & Espinoza, 2016; Segura et al., 2019; J. Sulca et al., 2018).

6. Conclusions

We compared and evaluated the performance of 30 GCM-RCM simulations within the framework of CORDEX-SAM and Eta RCM in representing the precipitation spatio-temporal climatological features and interannual variability during the "historical" period (1981–2005). These simulations result from combination of 6 RCMs and 10 GCMs at spatial resolutions ranging from 0.2° to 0.5°. The results reveal a mixed performance, with some aspects well-reproduced such as the spatial behavior of seasonality. However, most RCM simulations struggled to accurately replicate the spatial patterns of orographic rainfall, and no model excelled in capturing the spatial features of interannual rainfall variability observed in the period between 1981 and 2005.

In this set of simulations, the best performance is observed in simulations with the finest spatial resolution when it comes to reproducing orographic precipitation over the Andes-Amazon transition region (specifically, the Eta RCM at 0.2° × 0.2° resolution). However, it is noteworthy that simulations with a grid size of 0.22° may underperform in comparison to coarser grid-size (ranging from 0.44° to 0.5°) simulations in simulating various orographic precipitation features. For example, excessive overestimations reaching as much as 2,500% are reached by the S22 RC47 simulations in some Andes-Amazon transition region locations. These wet biases are more pronounced during the rainiest months; and, in the lowlands, precipitation can be overestimated by as much as 100%, especially at equatorial-most regions.

Addressing these biases in future GCM dynamical downscaling efforts for this region will require consideration of convection-permitting scales and the selection of an appropriate, high-resolution adapted physical parameterization setup. Further development in these areas is essential to improve the simulation of intricate interactions between local terrain and tropical rainfall regimes in this complex region.

Finally, the results of this study offer valuable insights that can enhance the application of this set of regional climate simulations for both climate and non-climate scientists engaged in vulnerability and impact studies at the local scale under future climate scenarios (Figures 11 and 12). Future research should focus on a process-oriented approach to identify sub-monthly (e.g., synoptic) mechanisms leading to model biases. This, in turn, can lead to the improvement of bias correction techniques (e.g., Maraun et al., 2021). Such approaches would serve in order to project future scenarios related to local hydrometeorological risks (e.g., Figueroa et al., 2020; Valenzuela et al., 2023).

Data Availability Statement

The precipitation gridded datasets used in this paper were acquired from the Climate Hazards Group (CHIRPS, https://chc.ucsb.edu/data/chirps/) and German Research Center for Geosciences (RAIN4PE, https://datapub.gfz-potsdam.de/download/10.5880.PIK.2020.010enouiv/). The CORDEX-SAM and Eta RCM's data are publicly available and can be downloaded from the Earth System Grid Federation (ESGF) portals (https://esgf-data.dkrz.de/search/esgf-dkrz/). The GTOPO30 dataset is available at the U.S. Geological Survey site (https://www.usgs.gov/centers/eros/science/usgs-eros-archive-digital-elevation-global-30-arc-second-elevation-gtopo30).

Acknowledgments
We thank three anonymous reviewers for their helpful comments, which helped us enrich the discussions of our study and improve the quality and clarity of the manuscript. This research was funded by the No. 77-2021-FONDECYT/BM Project and J.-C.E. received the support of the French AMANECER-MOPGA project funded by ANR and IRD (ref. ANR-18-MPGA-0008). We also acknowledge the contribution of project ACE-Amazon funded by the regional program CLIMAT-AmSud (21-CLIMAT-01). Thanks to Livia Dutra (Universidade de São Paulo) and Daniela Carneiro (Instituto Nacional de Pesquisas Espaciais) for providing the orography fields of the RegCM4.3 and the Eta models, respectively.

References

Adler, C., Wester, P., Bhatt, I., Huggel, C., Insarov, G. E., Morecroft, M. D., et al. (2022). Cross-chapter paper 5: Mountains. In H.-O. Pörtner, D. C. Roberts, M. Tignor, E. S. Poloczanska, K. Mintenbeck, A. Alegría, et al. (Eds.), *Climate change 2022: Impacts, adaptation and vulnerability. Contribution of Working Group II to the sixth assessment report of the intergovernmental panel on climate change*(pp. 2273–2318). Cambridge University Press. https://doi.org/10.1017/9781009325844.022

Almazroui, M., Ashfaq, M., Islam, M. N., Rashid, I. U., Kamil, S., Abid, M. A., et al. (2021). Assessment of CMIP6 performance and projected temperature and precipitation changes over South America. *Earth Systems and Environment*, *5*(2), 155–183. https://doi.org/10.1007/s41748-021-00233-6

Ambrizzi, T., Reboita, M. S., da Rocha, R. P., & Llopart, M. (2019). The state of the art and fundamental aspects of regional climate modeling in South America. *Annals of the New York Academy of Sciences*, *1436*(1), 98–120. https://doi.org/10.1111/nyas.13932

Arias, P. A., Garreaud, R., Poveda, G., Espinoza, J. C., Molina-Carpio, J., Masiokas, M., et al. (2021). Hydroclimate of the Andes Part II: Hydroclimate variability and sub-continental patterns. *Frontiers in Earth Science*, *8*, 505467. https://doi.org/10.3389/feart.2020.505467

Armijos, E., Crave, A., Espinoza, J. C., Filizola, N., Espinoza-Villar, R., Ayes, et al. (2020). Rainfall control on Amazon sediment flux: Synthesis from 20 years of monitoring. *Environmental Research Communications*, *2*(5), 051008. https://doi.org/10.1088/2515-7620/ab9003

Bentsen, M., Bethke, I., Debernard, J. B., Iversen, T., Kirkevåg, A., Seland, Ø., et al. (2013). The Norwegian Earth system model, NorESM1-M—Part 1: Description and basic evaluation of the physical climate. *Geoscientific Model Development*, *6*(3), 687–720. https://doi.org/10.5194/gmd-6-687-2013

Blázquez, J., & Solman, S. A. (2020). Multiscale precipitation variability and extremes over South America: Analysis of future changes from a set of CORDEX regional climate model simulations. *Climate Dynamics*, *55*(7–8), 2089–2106. https://doi.org/10.1007/s00382-020-05370-8

Boulton, C. A., Lenton, T. M., & Boers, N. (2022). Pronounced loss of Amazon rainforest resilience since the early 2000s. *Nature Climate Change*, *12*(3), 271–278. https://doi.org/10.1038/s41558-022-01287-8

Bozkurt, D., Rojas, M., Boisier, J. P., Rondanelli, R., Garreaud, R., & Gallardo, L. (2019). Dynamical downscaling over the complex terrain of southwest South America: Present climate conditions and added value analysis. *Climate Dynamics*, *53*(11), 6745–6767. https://doi.org/10.1007/s00382-019-04959-y

Cazorla, M., Gallardo, L., & Jimenez, R. (2022). The complex Andes region needs improved efforts to face climate extremes. *Elementa: Science of the Anthropocene*, *10*(1), 00092. https://doi.org/10.1525/elementa.2022.00092

Chavez, S. P., & Takahashi, K. (2017). Orographic rainfall hotspots in the Andes-Amazon transition according to the TRMM precipitation radar and in situ data. *Journal of Geophysical Research: Atmospheres*, *122*(11), 5870–5882. https://doi.org/10.1002/2016JD026282

Chimborazo, O., & Vuille, M. (2021). Present-day climate and projected future temperature and precipitation changes in Ecuador. *Theoretical and Applied Climatology*, *143*(3–4), 1581–1597. https://doi.org/10.1007/s00704-020-03483-y

Chou, S. C., Lyra, A., Mourão, C., Dereczynski, C., Pilotto, I., Gomes, J., et al. (2014). Evaluation of the Eta simulations nested in three global climate models. *American Journal of Climate Change*, *03*(05), 438–454. https://doi.org/10.4236/ajcc.2014.35039

Collins, W. J., Bellouin, N., Doutriaux-Boucher, M., Gedney, N., Halloran, P., Hinton, T., et al. (2011). Development and evaluation of an Earth-System model—HadGEM2. *Geoscientific Model Development*, *4*(4), 1051–1075. https://doi.org/10.5194/gmd-4-1051-2011

Condom, T., Martínez, R., Pabón, J. D., Costa, F., Pineda, L., Nieto, J. J., et al. (2020). Climatological and hydrological observations for the South American Andes: In situ stations, satellite, and reanalysis data sets. *Frontiers in Earth Science*, *8*, 92. https://doi.org/10.3389/feart.2020.00092

Doblas-Reyes, F. J., Sörensson, A. A., Almazroui, M., Dosio, A., Gutowski, W. J., Haarsma, R., et al. (2021). Linking global to regional climate change. In V. Masson-Delmotte, P. Zhai, A. Pirani, S. L. Connors, C. Péan, S. Berger, et al. (Eds.), *Climate change 2021: The physical science basis. Contribution of Working Group I to the sixth assessment report of the Intergovernmental Panel on Climate Change* (pp. 1363–1512). Cambridge University Press. https://doi.org/10.1017/9781009157896.012

Dufresne, J.-L., Foujols, M.-A., Denvil, S., Caubel, A., Marti, O., Aumont, O., et al. (2013). Climate change projections using the IPSL-CM5 Earth system model: From CMIP3 to CMIP5. *Climate Dynamics*, *40*(9–10), 2123–2165. https://doi.org/10.1007/s00382-012-1636-1

Dunne, J. P., John, J. G., Adcroft, A. J., Griffies, S. M., Hallberg, R. W., Shevliakova, E., et al. (2012). GFDL's ESM2 global coupled climate–carbon Earth system models. Part I: Physical formulation and baseline simulation characteristics. *Journal of Climate*, *25*(19), 6646–6665. https://doi.org/10.1175/JCLI-D-11-00560.1

Earth Resources Observation and Science Center. (2018). Global 30 arc-second elevation (GTOPO30) [Dataset]. United States Geological Survey, *11*, 40. Retrieved from https://www.usgs.gov/centers/eros/science/usgs-eros-archive-digital-elevation-global-30-arc-second-elevation-gtopo30

Eghdami, M., & Barros, A. P. (2020). Deforestation impacts on orographic precipitation in the tropical Andes. *Frontiers in Environmental Science*, *8*, 580159. https://doi.org/10.3389/fenvs.2020.580159

Espinoza, J. C., Chavez, S., Ronchail, J., Junquas, C., Takahashi, K., & Lavado, W. (2015). Rainfall hotspots over the southern tropical Andes: Spatial distribution, rainfall intensity, and relations with large-scale atmospheric circulation: Rainfall hotspots over the southern tropical Andes. *Water Resources Research*, *51*(5), 3459–3475. https://doi.org/10.1002/2014WR016273

Espinoza, J. C., Garreaud, R., Poveda, G., Arias, P. A., Molina-Carpio, J., Masiokas, M., et al. (2020). Hydroclimate of the Andes Part I: Main climatic features. *Frontiers in Earth Science*, *8*, 64. https://doi.org/10.3389/feart.2020.00064

Espinoza, J. C., Ronchail, J., Guyot, J. L., Cochonneau, G., Naziano, F., Lavado, W., et al. (2009). Spatio-temporal rainfall variability in the Amazon basin countries (Brazil, Peru, Bolivia, Colombia, and Ecuador). *International Journal of Climatology*, *29*(11), 1574–1594. https://doi.org/10.1002/joc.1791

Espinoza, J. C., Ronchail, J., Marengo, J. A., & Segura, H. (2019). Contrasting North–South changes in Amazon wet-day and dry-day frequency and related atmospheric features (1981–2017). *Climate Dynamics*, *52*(9–10), 5413–5430. https://doi.org/10.1007/s00382-018-4462-2

Espinoza, J. C., Segura, H., Ronchail, J., Drapeau, G., & Gutierrez-Cori, O. (2016). Evolution of wet-day and dry-day frequency in the western Amazon basin: Relationship with atmospheric circulation and impacts on vegetation. *Water Resources Research*, *52*(11), 8546–8560. https://doi.org/10.1002/2016WR019305

Eyring, V., Bony, S., Meehl, G. A., Senior, C. A., Stevens, B., Stouffer, R. J., & Taylor, K. E. (2016). Overview of the Coupled Model Intercomparison Project Phase 6 (CMIP6) experimental design and organization. *Geoscientific Model Development*, *9*(5), 1937–1958. https://doi.org/10.5194/gmd-9-1937-2016

Falco, M., Carril, A. F., Menéndez, C. G., Zaninelli, P. G., & Li, L. Z. X. (2019). Assessment of CORDEX simulations over South America: Added value on seasonal climatology and resolution considerations. *Climate Dynamics*, *52*(7–8), 4771–4786. https://doi.org/10.1007/s00382-018-4412-z

Fassoni-Andrade, A. C., Fleischmann, A. S., Papa, F., Paiva, R. C. D. D., Wongchuig, S., Melack, J. M., et al. (2021). Amazon hydrology from space: Scientific advances and future challenges. *Reviews of Geophysics*, *59*(4), 97. https://doi.org/10.1029/2020RG000728

Fernández-Palomino, C. A., Hattermann, F. F., Krysanova, V., Lobanova, A., Vega-Jácome, F., Lavado, W., et al. (2022). A novel high-resolution gridded precipitation dataset for Peruvian and Ecuadorian watersheds: Development and hydrological evaluation [Dataset]. Journal of Hydrometeorology, *23*(3), 309–336. https://doi.org/10.1175/JHM-D-20-0285.1

Figueroa, M., Armijos, E., Espinoza, J. C., Ronchail, J., & Fraizy, P. (2020). On the relationship between reversal of the river stage (repiquetes), rainfall and low-level wind regimes over the western Amazon basin. *Journal of Hydrology: Regional Studies*, *32*, 100752. https://doi.org/10.1016/j.ejrh.2020.100752

Flores-Rojas, J. L., Moya-Álvarez, A. S., Valdivia-Prado, J. M., Piñas-Laura, M., Kumar, S., Karam, H. A., et al. (2021). On the dynamic mechanisms of intense rainfall events in the central Andes of Peru, Mantaro valley. *Atmospheric Research*, *248*, 105188. https://doi.org/10.1016/j.atmosres.2020.105188

Funk, C., Peterson, P., Landsfeld, M., Pedreros, D., Verdin, J., Shukla, S., et al. (2015). The climate hazards infrared precipitation with stations—A new environmental record for monitoring extremes [Dataset]. Scientific Data, *2*(1), 150066. https://doi.org/10.1038/sdata.2015.66

Garreaud, R. D. (2009). The Andes climate and weather. *Advances in Geosciences*, *22*, 3–11. https://doi.org/10.5194/adgeo-22-3-2009

Gibson, P. B., Waliser, D. E., Lee, H., Tian, B., & Massoud, E. (2019). Climate model evaluation in the presence of observational uncertainty: Precipitation indices over the contiguous United States. *Journal of Hydrometeorology*, *20*(7), 1339–1357. https://doi.org/10.1175/JHM-D-18-0230.1

Giorgi, F., Coppola, E., Solmon, F., Mariotti, L., Sylla, M., Bi, X., et al. (2012). RegCM4: Model description and preliminary tests over multiple CORDEX domains. *Climate Research*, *52*, 7–29. https://doi.org/10.3354/cr01018

Giorgi, F., & Gutowski, W. J. (2015). Regional dynamical downscaling and the CORDEX initiative. *Annual Review of Environment and Resources*, *40*(1), 467–490. https://doi.org/10.1146/annurev-environ-102014-021217

Gomez-Rios, S., Zuluaga, M. D., & Hoyos, C. D. (2023). Orographic controls over convection in an Inter-Andean valley in northern South America. *Monthly Weather Review*, *151*(1), 145–162. https://doi.org/10.1175/MWR-D-21-0231.1

Haghtalab, N., Moore, N., Heerspink, B. P., & Hyndman, D. W. (2020). Evaluating spatial patterns in precipitation trends across the Amazon basin driven by land cover and global scale forcings. *Theoretical and Applied Climatology*, *140*(1–2), 411–427. https://doi.org/10.1007/s00704-019-03085-3

Hazeleger, W., Severijns, C., Semmler, T., Ştefănescu, S., Yang, S., Wang, X., et al. (2010). EC-Earth: A seamless earth-system prediction approach in action. *Bulletin of the American Meteorological Society*, *91*(10), 1357–1364. https://doi.org/10.1175/2010BAMS2877.1

Hoorn, C., Wesselingh, F. P., ter Steege, H., Bermudez, M. A., Mora, A., Sevink, J., et al. (2010). Amazonia through time: Andean uplift, climate change, landscape evolution, and biodiversity. *Science*, *330*(6006), 927–931. https://doi.org/10.1126/science.1194585

Jacob, D., Elizalde, A., Haensler, A., Hagemann, S., Kumar, P., Podzun, R., et al. (2012). Assessing the transferability of the regional climate model REMO to different COordinated Regional Climate Downscaling EXperiment (CORDEX) regions. *Atmosphere*, *3*(1), 181–199. https://doi.org/10.3390/atmos3010181

Junquas, C., Heredia, M. B., Condom, T., Ruiz-Hernández, J. C., Campozano, L., Dudhia, J., et al. (2022). Regional climate modeling of the diurnal cycle of precipitation and associated atmospheric circulation patterns over an Andean glacier region (Antisana, Ecuador). *Climate Dynamics*, *58*(11–12), 3075–3104. https://doi.org/10.1007/s00382-021-06079-y

Junquas, C., Takahashi, K., Condom, T., Espinoza, J.-C., Chavez, S., Sicart, J.-E., & Lebel, T. (2018). Understanding the influence of orography on the precipitation diurnal cycle and the associated atmospheric processes in the central Andes. *Climate Dynamics*, *50*(11–12), 3995–4017. https://doi.org/10.1007/s00382-017-3858-8

Kendon, E. J., Prein, A. F., Senior, C. A., & Stirling, A. (2021). Challenges and outlook for convection-permitting climate modelling. *Philosophical Transactions of the Royal Society A: Mathematical, Physical & Engineering Sciences*, *379*(2195), 20190547. https://doi.org/10.1098/rsta.2019.0547

Laraque, A., Ronchail, J., Cochonneau, G., Pombosa, R., & Guyot, J. L. (2007). Heterogeneous distribution of rainfall and discharge regimes in the Ecuadorian Amazon basin. *Journal of Hydrometeorology*, *8*(6), 1364–1381. https://doi.org/10.1175/2007JHM784.1

Lavado-Casimiro, W., & Espinoza, J. C. (2014). Impactos de El Niño y La Niña en las lluvias del Perú (1965–2007). *Revista Brasileira de Meteorologia*, *29*(2), 171–182. https://doi.org/10.1590/S0102-77862014000200003

Lavado-Casimiro, W. S., Felipe, O., Silvestre, E., & Bourrel, L. (2013). ENSO impact on hydrology in Peru. *Advances in Geosciences*, *33*, 33–39. https://doi.org/10.5194/adgeo-33-33-2013

Llopart, M., Reboita, M. S., & da Rocha, R. P. (2019). Assessment of multi-model climate projections of water resources over South America CORDEX domain. *Climate Dynamics*, *54*(1–2), 99–116. https://doi.org/10.1007/s00382-019-04990-z

Lucas-Picher, P., Laprise, R., & Winger, K. (2017). Evidence of added value in North American regional climate model hindcast simulations using ever-increasing horizontal resolutions. *Climate Dynamics*, *48*(7–8), 2611–2633. https://doi.org/10.1007/s00382-016-3227-z

Maraun, D., Truhetz, H., & Schaffer, A. (2021). Regional climate model biases, their dependence on synoptic circulation biases and the potential for bias adjustment: A process-oriented evaluation of the Austrian regional climate projections. *Journal of Geophysical Research: Atmospheres*, *126*(6), e2020JD032824. https://doi.org/10.1029/2020JD032824

Marengo, J. A., & Espinoza, J. C. (2016). Extreme seasonal droughts and floods in Amazonia: Causes, trends and impacts. *International Journal of Climatology*, *36*(3), 1033–1050. https://doi.org/10.1002/joc.4420

Marengo, J. A., Souza, C. M., Thonicke, K., Burton, C., Halladay, K., Betts, R. A., et al. (2018). Changes in climate and land use over the Amazon region: Current and future variability and trends. *Frontiers in Earth Science*, *6*, 228. https://doi.org/10.3389/feart.2018.00228

Mascaro, G., Viola, F., & Deidda, R. (2018). Evaluation of precipitation from EURO-CORDEX regional climate simulations in a small-scale Mediterranean site. *Journal of Geophysical Research: Atmospheres*, *123*(3), 1604–1625. https://doi.org/10.1002/2017JD027463

Meehl, G. A., Covey, C., Delworth, T., Latif, M., McAvaney, B., Mitchell, J. F. B., et al. (2007). THE WCRP CMIP3 multimodel dataset: A new era in climate change research. *Bulletin of the American Meteorological Society*, *88*(9), 1383–1394. https://doi.org/10.1175/BAMS-88-9-1383

Menéndez, C., Zaninelli, P., Carril, A., & Sánchez, E. (2016). Hydrological cycle, temperature, and land surface-atmosphere interaction in the La Plata basin during summer: Response to climate change. *Climate Research*, *68*(2–3), 231–241. https://doi.org/10.3354/cr01373

Mesinger, F., Chou, S. C., Gomes, J. L., Jovic, D., Bastos, P., Bustamante, J. F., et al. (2012). An upgraded version of the Eta model. *Meteorology and Atmospheric Physics*, *116*(3–4), 63–79. https://doi.org/10.1007/s00703-012-0182-z

Moya-Álvarez, A. S., Martínez-Castro, D., Kumar, S., Estevan, R., & Silva, Y. (2019). Response of the WRF model to different resolutions in the rainfall forecast over the complex Peruvian orography. *Theoretical and Applied Climatology*, *137*(3), 2993–3007. https://doi.org/10.1007/s00704-019-02782-3

Newell, F. L., Ausprey, I. J., & Robinson, S. K. (2022). Spatiotemporal climate variability in the Andes of northern Peru: Evaluation of gridded datasets to describe cloud forest microclimate and local rainfall. *International Journal of Climatology*, *42*(11), 5892–5915. https://doi.org/10.1002/joc.7567

Nobre, C. A., Sampaio, G., Borma, L. S., Castilla-Rubio, J. C., Silva, J. S., & Cardoso, M. (2016). Land-use and climate change risks in the Amazon and the need of a novel sustainable development paradigm. *Proceedings of the National Academy of Sciences*, *113*(39), 10759–10768. https://doi.org/10.1073/pnas.1605516113

Ochoa, A., Campozano, L., Sánchez, E., Gualán, R., & Samaniego, E. (2016). Evaluation of downscaled estimates of monthly temperature and precipitation for a Southern Ecuador case study. *International Journal of Climatology*, *36*(3), 1244–1255. https://doi.org/10.1002/joc.4418

Ometto, J. P., Kalaba, K., Anshari, G. Z., Chacón, N., Farrell, A., Halim, S. A., et al. (2022). Cross-chapter paper 7: Tropical forests. In H.-O. Pörtner, D. C. Roberts, M. Tignor, E. S. Poloczanska, K. Mintenbeck, A. Alegría, et al. (Eds.), *Climate change 2022: Impacts, adaptation and vulnerability. Contribution of Working Group II to the sixth assessment report of the Intergovernmental Panel on Climate Change* (pp. 2369–2410). Cambridge University Press. https://doi.org/10.1017/9781009325844.024

Ortega, G., Arias, P. A., Villegas, J. C., Marquet, P. A., & Nobre, P. (2021). Present-day and future climate over central and South America according to CMIP5/CMIP6 models. *International Journal of Climatology*, *41*(15), 6713–6735. https://doi.org/10.1002/joc.7221

Pabón-Caicedo, J. D., Arias, P. A., Carril, A. F., Espinoza, J. C., Borrel, L. F., Goubanova, K., et al. (2020). Observed and projected hydroclimate changes in the Andes. *Frontiers in Earth Science*, *8*, 61. https://doi.org/10.3389/feart.2020.00061

Pörtner, H.-O., Roberts, D. C., Adams, H., Adelekan, I., Adler, C., Adrian, R., et al. (2022). Technical Summary. In H.-O. Pörtner, D. C. Roberts, M. Tignor, E. S. Poloczanska, K. Mintenbeck, M. Tignor, et al. (Eds.), *Climate change 2022: Impacts, adaptation and vulnerability. Contribution of Working Group II to the sixth assessment report of the Intergovernmental Panel on Climate Change* (pp. 37–118). Cambridge University Press. https://doi.org/10.1017/9781009325844.002

Prein, A. F., Gobiet, A., Truhetz, H., Keuler, K., Goergen, K., Teichmann, C., et al. (2016). Precipitation in the EURO-CORDEX 0.11° and 0.44° simulations: High resolution, high benefits? *Climate Dynamics*, *46*(1–2), 383–412. https://doi.org/10.1007/s00382-015-2589-y

Reboita, M. S., da Rocha, R. P., de Souza, C. A., Baldoni, T. C., da Silva, P. L. L. S., & Ferreira, G. W. S. (2022). Future projections of extreme precipitation climate indices over South America based on CORDEX-CORE multimodel ensemble. *Atmosphere*, *13*(9), 1463. https://doi.org/10.3390/atmos13091463

Rosales, A. G., Junquas, C., Da Rocha, R. P., Condom, T., & Espinoza, J.-C. (2022). Valley–mountain circulation associated with the diurnal cycle of precipitation in the tropical Andes (Santa River Basin, Peru). *Atmosphere*, *13*(2), 344. https://doi.org/10.3390/atmos13020344

Rotstayn, L. D., Collier, M. A., Dix, M. R., Feng, Y., Gordon, H. B., Ofarrell, S. P., et al. (2009). Improved simulation of Australian climate and ENSO-related rainfall variability in a global climate model with an interactive aerosol treatment. *International Journal of Climatology*, *30*(7), 1067–1088. https://doi.org/10.1002/joc.1952

Samuelsson, P., Gollvik, S., Jansson, C., Kupiainen, M., Kourzeneva, E., & van de Berg, W. M. (2015). *The surface processes of the Rossby Centre regional atmospheric climate model (RCA4)*. SMHI. Retrieved from http://urn.kb.se/resolve?urn=urn:nbn:se:smhi:diva-2840

Samuelsson, P., Jones, C. G., Willén, U., Ullerstig, A., Gollvik, S., Hansson, U., et al. (2011). The Rossby Centre regional climate model RCA3: Model description and performance. *Tellus A: Dynamic Meteorology and Oceanography*, *63*(1), 4. https://doi.org/10.1111/j.1600-0870.2010.00478.x

Segura, H., Junquas, C., Espinoza, J. C., Vuille, M., Jauregui, Y. R., Rabatel, A., et al. (2019). New insights into the rainfall variability in the tropical Andes on seasonal and interannual time scales. *Climate Dynamics*, *53*(1–2), 405–426. https://doi.org/10.1007/s00382-018-4590-8

Sierra, J. P., Junquas, C., Espinoza, J. C., Segura, H., Condom, T., Andrade, M., et al. (2022). Deforestation impacts on Amazon-Andes hydroclimatic connectivity. *Climate Dynamics*, *58*(9–10), 2609–2636. https://doi.org/10.1007/s00382-021-06025-y

Skamarock, W. C., Klemp, J. B., Dudhia, J., Gill, D. O., Barker, D. M., Duda, M. G., et al. (2008). *A description of the advanced research WRF version 3, note NCAR/TN-475+ STR*. NCAR Tech Colorado. https://doi.org/10.5065/D68S4MVH

Solman, S. A., & Blázquez, J. (2019). Multiscale precipitation variability over South America: Analysis of the added value of CORDEX RCM simulations. *Climate Dynamics*, *53*(3–4), 1547–1565. https://doi.org/10.1007/s00382-019-04689-1

Staal, A., Tuinenburg, O. A., Bosmans, J. H. C., Holmgren, M., van Nes, E. H., Scheffer, M., et al. (2018). Forest-rainfall cascades buffer against drought across the Amazon. *Nature Climate Change*, *8*(6), 539–543. https://doi.org/10.1038/s41558-018-0177-y

Sulca, J., Takahashi, K., Espinoza, J.-C., Vuille, M., & Lavado-Casimiro, W. (2018). Impacts of different ENSO flavors and tropical Pacific convection variability (ITCZ, SPCZ) on austral summer rainfall in South America, with a focus on Peru. *International Journal of Climatology*, *38*(1), 420–435. https://doi.org/10.1002/joc.5185

Sulca, J. C., & da Rocha, R. P. (2021). Influence of the coupling South Atlantic Convergence Zone-El Niño-Southern Oscillation (SACZ-ENSO) on the projected precipitation changes over the central Andes. *Climate*, *9*(5), 77. https://doi.org/10.3390/cli9050077

Taylor, K. E. (2001). Summarizing multiple aspects of model performance in a single diagram. *Journal of Geophysical Research*, *106*(D7), 7183–7192. https://doi.org/10.1029/2000JD900719

Taylor, K. E., Stouffer, R. J., & Meehl, G. A. (2012). An overview of CMIP5 and the experiment design. *Bulletin of the American Meteorological Society*, *93*(4), 485–498. https://doi.org/10.1175/BAMS-D-11-00094.1

Torma, C., Giorgi, F., & Coppola, E. (2015). Added value of regional climate modeling over areas characterized by complex terrain-precipitation over the Alps. *Journal of Geophysical Research: Atmospheres*, *120*(9), 3957–3972. https://doi.org/10.1002/2014JD022781

Valenzuela, J., Figueroa, M., Armijos, E., Espinoza, J.-C., Wongchuig, S., & Ramirez-Avila, J. J. (2023). Flooding risk of cropland areas by repiquetes in the western Amazon basin: A case study of Peruvian Tamshiyacu City. *Journal of Hydrology: Regional Studies*, *47*, 101428. https://doi.org/10.1016/j.ejrh.2023.101428

Vera, C., Higgins, W., Amador, J., Ambrizzi, T., Garreaud, R., Gochis, D., et al. (2006). Toward a unified view of the American Monsoon systems. *Journal of Climate*, *19*(20), 4977–5000. https://doi.org/10.1175/JCLI3896.1

Voldoire, A., Sanchez-Gomez, E., Salas y Mélia, D., Decharme, B., Cassou, C., Sénési, S., et al. (2013). The CNRM-CM5.1 global climate model: Description and basic evaluation. *Climate Dynamics*, *40*(9–10), 2091–2121. https://doi.org/10.1007/s00382-011-1259-y

von Salzen, K., Scinocca, J. F., McFarlane, N. A., Li, J., Cole, J. N. S., Plummer, D., et al. (2013). The Canadian fourth generation atmospheric global climate model (CanAM4). Part I: Representation of physical processes. *Atmosphere-Ocean*, *51*(1), 104–125. https://doi.org/10.1080/07055900.2012.755610

Vuille, M., Carey, M., Huggel, C., Buytaert, W., Rabatel, A., Jacobsen, D., et al. (2018). Rapid decline of snow and ice in the tropical Andes—Impacts, uncertainties and challenges ahead. *Earth-Science Reviews*, *176*, 195–213. https://doi.org/10.1016/j.earscirev.2017.09.019

Watanabe, M., Suzuki, T., Oishi, R., Komuro, Y., Watanabe, S., Emori, S., et al. (2010). Improved climate simulation by MIROC5: Mean states, variability, and climate sensitivity. *Journal of Climate*, *23*(23), 6312–6335. https://doi.org/10.1175/2010JCLI3679.1

Young, B., Young, K. R., & Josse, C. (2011). Vulnerability of tropical Andean ecosystems to climate change. In S. K. Herzog, R. Martínez, P. M. Jorgensen, & H. Tiessen (Eds.), *Climate change and biodiversity in the tropical Andes* (pp. 170–181). Inter American Institute for Global Change Research (IAI)—Scientific Committee on Problems of the Environment (SCOPE).

Zanchettin, D., Rubino, A., Matei, D., Bothe, O., & Jungclaus, J. H. (2013). Multidecadal-to-centennial SST variability in the MPI-ESM simulation ensemble for the last millennium. *Climate Dynamics*, *40*(5–6), 1301–1318. https://doi.org/10.1007/s00382-012-1361-9